JACS
JOURNAL OF THE AMERICAN CHEMICAL SOCIETY

Article

pubs.acs.org/JACS

Proton-Based Structural Analysis of a Heptahelical Transmembrane Protein in Lipid Bilayers

Daniela Lalli,[†] Matthew N. Idso,[‡] Loren B. Andreas,[†,∥] Sunyia Hussain,[‡] Naomi Baxter,[§] Songi Han,[‡,§] Bradley F. Chmelka,*[,‡] and Guido Pintacuda*[,†]

[†]Centre de RMN à Très Hauts Champs, Institut des Sciences Analytiques (UMR 5280 - CNRS, ENS Lyon, UCB Lyon 1), Université de Lyon, 69100 Villeurbanne, France

[‡]Department of Chemical Engineering, University of California, Santa Barbara, California 93106, United States

[§]Department of Chemistry and Biochemistry, University of California, Santa Barbara, California 93106, United States

Supporting Information

ABSTRACT: The structures and properties of membrane proteins in lipid bilayers are expected to closely resemble those in native cell-membrane environments, although they have been difficult to elucidate. By performing solid-state NMR measurements at very fast (100 kHz) magic-angle spinning rates and at high (23.5 T) magnetic field, severe sensitivity and resolution challenges are overcome, enabling the atomic-level characterization of membrane proteins in lipid environments. This is demonstrated by extensive ^{1}H-based resonance assignments of the fully protonated heptahelical membrane protein proteorhodopsin, and the efficient identification of numerous ^{1}H−^{1}H dipolar interactions, which provide distance constraints, inter-residue proximities, relative orientations of secondary structural elements, and protein−cofactor interactions in the hydrophobic transmembrane regions. These results establish a general approach for high-resolution structural studies of membrane proteins in lipid environments via solid-state NMR.

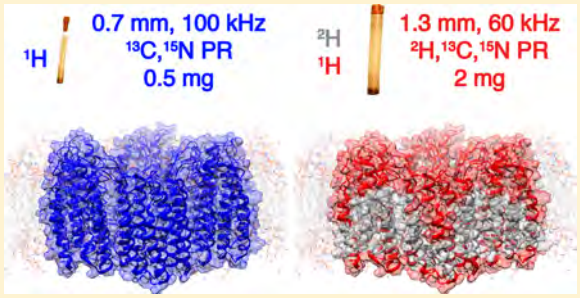

INTRODUCTION

Atomic level characterization of membrane proteins in lipid bilayers is essential for understanding their functions, although extremely challenging. Membrane proteins in lipid environments generally lack long-range order, and tumble slowly in solutions, which respectively render scattering investigations infeasible and jeopardize liquid-state NMR investigations. Magic-angle spinning (MAS) solid-state NMR spectroscopy is a powerful tool that can reveal both structural and dynamical details of such systems,[1] yet its application has been limited by low spectral sensitivity and resolution, as well as by the difficulty in obtaining large (~20 mg) quantities of isotopically labeled proteins.

Many strategies have been employed to overcome the resolution and sensitivity issues that impede structural characterization of membrane proteins by MAS NMR. Proton detection is a powerful technique that exploits the high gyromagnetic ratio and abundance of proton nuclei to enhance the spectral sensitivity.[2] However, despite encouraging proof-of-principle studies performed on fully protonated model systems,[3] applications of ^{1}H-detection to membrane proteins in native-like lipid environments have been hindered by the low ^{1}H spectral resolution under moderate MAS rates (<40 kHz). Higher spectral resolution[4] can be achieved in part by proton dilution strategies (typically perdeuteration and back-protonation at the exchangeable sites) to quench the ^{1}H−^{1}H dipolar couplings that broaden NMR signals.[5] This strategy, however, is problematic during protein expression, due to anemic growth in deuterium oxide which sometimes is even incompatible with protein expression, as for example in mammalian cells. When feasible, it allows reintroduction of ^{1}H species exclusively at sites that are exchangeable and accessible to solvent, which notably do not include the extensive hydrophobic transmembrane regions, thereby precluding their analyses by ^{1}H-detected spectroscopy.[6] Unfolding and refolding membrane proteins leads to the introduction of ^{1}H species at the exchangeable sites of transmembrane regions, however such protocols are not general, and specific examples are rare.[1l,5d,7] To address this in part, isotopic labeling strategies have been developed in which membrane proteins are expressed in H_2O in the presence of deuterated ^{13}C glucose, such that ^{1}H/^{2}H species are homogeneously distributed in both water-accessible and inaccessible regions.[8] Nevertheless, in such cases the ^{1}H/^{2}H isotopomeric distributions often result in poorly resolved ^{13}C resonances from side-chain moieties that are crucial for structure determination.

The advent of MAS NMR probes capable of spinning at rates of 100 kHz or greater has reduced the amount of sample required,[2,5e,f,9] and, most importantly, reduced the need for

Received: May 24, 2017
Published: July 20, 2017

DOI: 10.1021/jacs.7b05269
J. Am. Chem. Soc. 2017, 139, 13006−13012

proton dilution.[10] This has opened unprecedented opportunities for structural investigations of biosolids by using sensitive ^{1}H-detected methods,[10,11] with a dramatic reduction in homogeneous line broadening to improve the resolution of ^{1}H resonances. However, even at the fastest (~100 kHz) sample spinning rates and the highest magnetic fields (23.5 T) currently available, membrane proteins in lipid bilayers remain challenging to study by NMR (or other methods), because of their inherently heterogeneous lipid bilayer environments in which they are naturally diluted and which limit spectral resolution and signal sensitivity.

Transmembrane proteins, in particular, are incorporated into lipid bilayers and perform sensing, transport and enzymatic functions in support of cellular viability. One example is the green variant of proteorhodopsin, a light-activated H^{+}-ion pump of 240 residues that in solution has an archetypical heptahelical transmembrane protein structure with a retinal cofactor.[12] While the structure of monomeric proteorhodopsin in detergents has been determined by solution NMR (pdb code: 2L6X),[13] the structure of the protein in native-like lipid environments remains unknown. This is complicated further by the tendency of proteorhodopsin molecules in bilayers to assemble into pentamers and hexamers, which are thought to mediate protein function.[14] Conventional ^{13}C-detected MAS NMR methods have enabled the extensive assignment of backbone and side-chain ^{13}C and ^{15}N resonances of proteorhodopsin oligomers in lipids.[15] However, only a partial assignment of the solvent-exposed amide ^{1}H resonances was possible with ^{1}H-detected measurements on perdeuterated protein, due to incomplete solvent exchange.[6]

Here, we demonstrate very fast (100 kHz) MAS NMR to be a general approach for structural analyses of fully protonated membrane proteins in near-native lipid environments. Notably, we show that the use of fast 100 kHz MAS conditions expedites sequence-specific resonance assignments and facilitates the detection of ^{1}H−^{1}H proximities in hydrophobic transmembrane regions, which are essential features of protein structure and for their function.

EXPERIMENTAL SECTION

Sample Preparation. Expression of isotopically labeled proteorhodopsin was carried out as described by Ward et al.[6] with a few differences. Following overnight growth of *E. coli* cells in the 25 mL culture, the cells were pelleted by centrifugation at ~5000 rpm and resuspended in 75 mL of M9 minimal media with all labels present. Subsequently, the 75 mL culture was grown at 37 °C to an O.D.$_{600}$ of 1.0−1.5 (approximately 6 h) and then added to 925 mL of M9 media (all labels present). Protein expression was induced at an O.D.$_{600}$ of 0.8 by the addition of IPTG to a concentration of 1 mM and allowed to proceed for ~24 h at room temperature without shaking. Protein purification was carried out using methods described previously[14a] with a few modifications. Cells were lysed by a freeze fracture step with three freeze−thaw cycles using liquid nitrogen in addition to probe tip sonication and incubation with DNase, lysozyme, and $MgCl_2$. Then, the large cell fragments containing proteorhodopsin were pelleted by centrifugation at 5000 rpm and then washed with 250 mL of phosphate buffered solution (150 mM KCl and KH_2PO_4, pH ≈ 8.7) by repeatedly suspending the cell pellet in 40 mL of buffer, shaking the solution for 5 min, and pelleting cells by centrifugation. Subsequently, proteorhodopsin was extracted from lysed *E. coli* membranes by overnight incubation of the washed cell fragments in a phosphate buffered solution containing 4% (w/v) *n*-dodecyl-*β*,D-maltoside surfactant. Following the Ni-NTA resin binding, washing and elution steps,[2] the optical purities of the proteorhodopsin samples, as measured by the ratio of absorbances at 280 to 520 nm, typically ranged between 1.8 and 2.2. The concentration of proteorhodopsin was estimated based on the absorbance at 520 nm, using an extinction coefficient of 49 000 $M^{-1}cm^{-1}$. Proteorhodopsin was reconstituted into 1,2-dimyristoyl-*sn*-glycero-3-phosphate (DMPA) and 1,2-dimyristoyl-*sn*-glycero-3-phosphocholine (DMPC) liposomes using procedures described previously, except using a 10 mM HEPES buffer that was titrated to a pH 6.2 using dilute HCl.[15b]

NMR Spectroscopy. All experiments were carried out on a Bruker Avance III 1 GHz standard bore spectrometer operating at a static field of 23.4 T, equipped with a triple channel H, C, N, 0.7 mm probe, at a MAS rate $\omega_r/2\pi$ of 100 kHz. Sample temperature was maintained at about 305 K using a Bruker cooling unit with regulated N_2 gas directed at the rotor. The temperature of this gas measured just before reaching the sample was 280 K. Chemical shifts were referenced to adamantane (^{1}H signal at 1.87 ppm).

The nonselective pulses were set to 1.1 μs at 227 kHz rf-field amplitude (^{1}H), 5.5 μs at 45 kHz rf-field amplitude (^{15}N) and 3.1 μs at 81 kHz rf-field amplitude (^{13}C). The dipolar-based ^{15}N,^{1}H and ^{13}C,^{1}H CP-HSQC experiments (H)CH and (H)NH follow, with little modifications, those introduced by Rienstra and co-workers.[3b,5a] (H)NCAHA, (H)N(CO)CAHA, (H)CANH, (H)(CO)CA(CO)NH, and (H)CONH experiments were performed as described recently.[5d,11b] The irradiation schemes are displayed in Figure S1 of the Supporting Information, SI. The ^{1}H−^{15}N and ^{1}H−^{13}C cross-polarization (CP) were performed using a constant RF frequency applied to ^{15}N and ^{13}C of 40 kHz and a pulse linearly ramped from 90% to 100% of a maximum RF frequency of 130 kHz on ^{1}H. The ^{13}C−^{15}N CP was performed using a constant RF frequency of 60 kHz on ^{13}C and a 10% tangent ramp of 40 kHz on ^{15}N for 10 ms. Low power WALTZ-16 decoupling of 10 kHz was applied for heteronuclear decoupling. Swept low-power TPPM (slTPPM)[16] decoupling was used during ^{13}C, ^{15}N chemical shift evolution with a ^{1}H RF frequency of 25 kHz and a pulse-length duration of 20 μs. DIPSI-2 of $\gamma B_1/2\pi$ = 20 kHz was used for ^{13}C decoupling during acquisition due to the presence of homonuclear ^{13}C−^{13}C *J*-couplings. Suppression of solvent signals[4a] was applied using the MISSISSIPPI scheme[17] without the homospoil gradient for 200 ms. The interscan recycle delay was 1 s.

The (H)CCH experiment follows that reported recently.[10,11b] The composite ^{13}C pulses of 25 kHz were applied for the TOCSY mixing for 15 ms. In the 3D (H)CHH experiment, ^{1}H−^{1}H RFDR recoupling[16] was applied after the back-CP at a ^{1}H RF frequency of 200 kHz, for 1.4 ms. No loss of water from the sample was observed during the acquisition of the spectra. Spectra were apodized in each dimension with 60° to 90° shifted squared sine-bells ("qsine 3" or "qsine 2" in Bruker Topspin), and zero-filled to at least twice the number of points in the indirect dimensions. Where line widths are reported, no apodization was applied for the reported frequencies. Acquisition and processing parameters specific for each data set are summarized in Tables S2. Spectra were processed with Topspin3.5, and their analysis was performed using Cara. The resonance assignments for ^{1}H, ^{13}C, and ^{15}N nuclei are listed in Table S3.

RESULTS AND DISCUSSION

A dipolar-mediated 2D ^{1}H−^{15}N correlation spectrum (Figure 1, blue) of fully protonated U−[^{13}C,^{15}N] proteorhodopsin acquired at 100 kHz MAS shows highly resolved signals from the amide moieties of the protein backbone. These correlations have an average proton line width of 190 Hz fwhm that is significantly narrower than in a spectrum acquired on an identical sample at 60 kHz MAS rates in a 1.3 mm probe (Figure S2). Surprisingly, these spectra show comparable signal sensitivities (Figure S3), despite the significantly lower sample quantity (~0.5 mg, 0.7 mm rotor) at 100 kHz MAS, compared to 60 kHz MAS (~2.0 mg, 1.3 mm rotor). Deuterated proteorhodopsin reprotonated at the amide sites by exchange in 100% protonated buffers, yields enhanced resolution in a ^{1}H−^{15}N correlation spectrum (Figure 1, red) acquired under

DOI: 10.1021/jacs.7b05269
J. Am. Chem. Soc. 2017, 139, 13006−13012

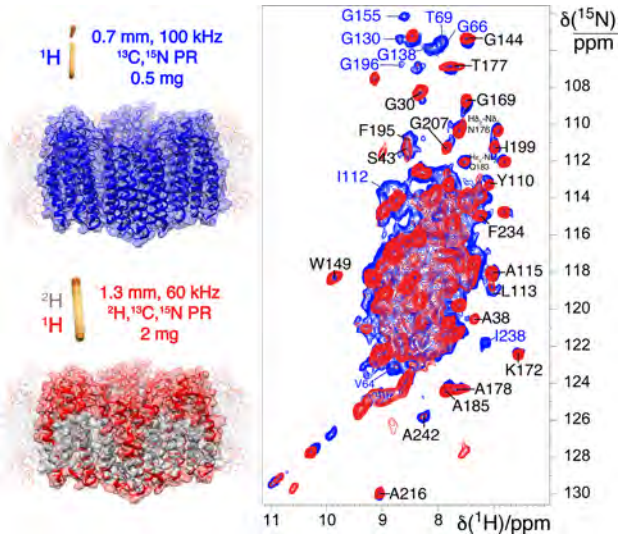

Figure 1. (A) Comparison of 2D ^{1}H−^{15}N CP-HSQC MAS NMR spectra acquired at 305 K on (blue trace) fully protonated U−[^{13}C,^{15}N] proteorhodopsin in DMPC:DMPA lipids at 100 kHz MAS, and (red trace) U−[^{2}H,^{15}N,^{13}C] proteorhodopsin, reprotonated in 100% protonated buffer, in the same lipids at 60 kHz MAS and a field strength of 23.5 T. (B) Schematic diagrams of proteorhodopsin oligomers, modeled from the monomeric protein structure (pdb code: 2L6X, see SI), in which residues with ^{1}H^{N} species are highlighted in blue and red for the fully protonated and perdeuterated samples, respectively.

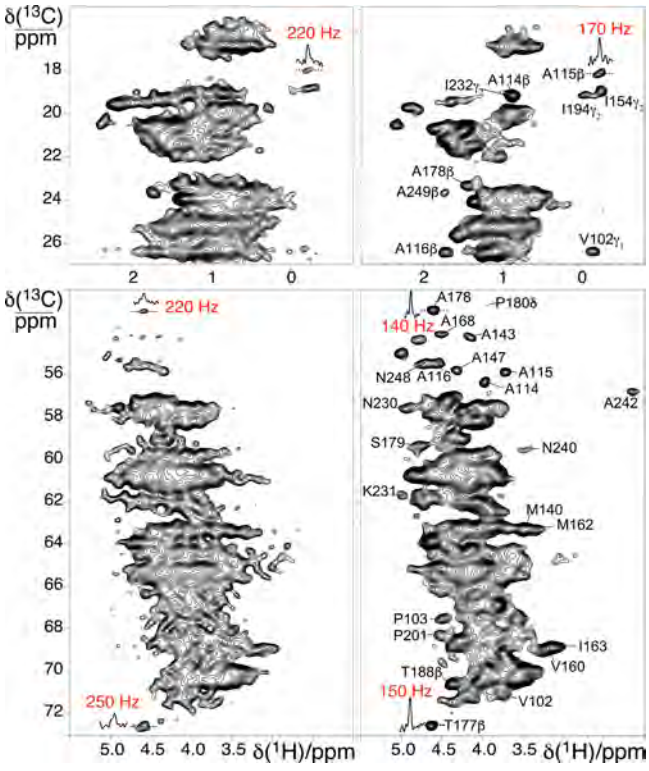

Figure 2. 2D ^{1}H−^{13}C CP-HSQC MAS NMR spectra acquired at 305 K and 23.5 T on fully protonated U−[^{13}C,^{15}N] proteorhodopsin in lipids at MAS rates of 60 kHz (left) and 100 kHz (right). The side chain and alpha regions of the spectra are shown in the top and bottom panels, respectively.

conventional 60 kHz MAS rates, showing average line widths of 140 Hz fwhm. However, the spectrum acquired on the perdeuterated sample at 60 kHz MAS has far fewer cross-peaks (Figure 1, red) than that from the fully protonated (Figure 1, blue) protein at 100 kHz MAS. This reflects an incomplete reintroduction of H^{N} species in perdeuterated proteorhodopsin, predominantly at residues in the hydrophobic transmembrane regions, which precludes their detection and structural analysis. By comparison, the ubiquity of ^{1}H species in fully protonated proteorhodopsin allows the entire biomolecule to be probed by ^{1}H-detected spectroscopy, in particular moieties on the aliphatic side-chains from which critical structural constraints are derived.

For example, the 2D ^{13}C−^{1}H CP-HSQC spectra of fully protonated proteorhodopsin at 60 kHz (Figure 2, left) and 100 kHz (Figure 2, right) MAS show correlated signals from ^{1}H and ^{13}C nuclei in the side-chains (top panel) and α positions (bottom panel). Substantially enhanced proton resolution is observed under the faster MAS conditions, as established by the larger number of fully resolved correlations that appear only in the spectrum recorded at 100 kHz; these include many ^{1}Hα resonances labeled in Figure 2, bottom panels, as well as ^{1}H methyl resonances (Figure 2, top panels). For several peaks resolved even at 60 kHz, the line widths are observed to be 50−100 Hz broader (Figure 2). The dramatic improvements in resolution enable the use of aliphatic side-chain protons as crucial reporters of protein structure. The significant increase in spectral resolution observed at 100 kHz MAS is surprising. While microcrystalline proteins, capsids, and fibrils often are homogeneous samples with rigid architectures that are amenable to MAS-averaging of homonuclear dipolar interactions, membrane proteins are less homogeneous, comparably flexible, and undergo a range of motions[18] that could reduce the benefits of faster MAS rates in improving signal resolution.

Nevertheless, in spectra from fully protonated proteorhodopsin in lipids, the average ^{1}H line width of ^{15}N−^{1}H correlations from amide moieties is ∼190 Hz fwhm at 100 kHz MAS, compared to ∼280 Hz fwhm at 60 kHz MAS. Greater resolution improvements are observed for aliphatic ^{1}H signals, where average line widths are approximately 145 Hz fwhm at 100 kHz MAS, versus about 235 Hz fwhm estimated from the few resolved signals at 60 kHz. The bulk ^{1}H coherence lifetimes were measured to be 2.5 ms on the fully protonated protein at 100 kHz MAS, which corresponds to residual homogeneous components of ∼125 Hz that suggest inhomogeneous line widths of 155 and 70 Hz for the ^{1}H^{N} and ^{1}Hα signals, respectively. The larger inhomogeneous components for the ^{1}H^{N} species likely arise from a distribution of hydrogen bonding environments, consistent with the larger range of amide ^{1}H^{N} shifts reported generally for proteins in the BMRB. The substantial homogeneous broadening remaining even at 100 kHz MAS conditions indicates that further narrowed ^{1}H line widths could be obtained for faster MAS rates and/or higher magnetic fields.[2,19]

Additionally, the ^{1}H signal resolution of fully protonated proteorhodopsin at 100 kHz MAS is comparable to that obtained with state-of-the-art partial isotopic labeling schemes. These labeling strategies, including fractional deuteration,[5h,20] isoleucine−leucine−valine labeling,[11,21] proton clouds,[5g] and stereospecific array isotopic labeling (SAIL),[22] selectively introduce ^{1}H side-chains into a deuterated protein matrix. Spectra of fully protonated proteorhodopsin in lipids at 100 kHz MAS show 20% higher ^{1}H resolution than for the similar α-helical transmembrane K^{+} channel Kcsa in lipid bilayers

DOI: 10.1021/jacs.7b05269
J. Am. Chem. Soc. 2017, 139, 13006−13012

labeled with an inverse fractional deuteration approach and using 60 kHz MAS rates.[8] Importantly, while this labeling scheme yields $^{1}H/^{2}H$ isotopomers that can account for up to 0.3 ppm dispersions in ^{13}C chemical shifts,[23] such effects are negligible in fully protonated proteins probed using 100 kHz MAS.

To facilitate rapid and global sequence-specific resonance assignments, judicious selections of 3D correlation experiments are essential for high sensitivity, in addition to high spectral resolution. Between the two different types of protein backbone ^{13}C species, the coherence lifetimes are longest for $^{13}C'$ species (T_2' = 21 ms, compared to $^{13}C\alpha$ T_2' = 12.5 ms, see Table S1), yielding considerable sensitivity advantages for 3D NMR measurements that rely on evolution of $^{13}C'$ versus $^{13}C\alpha$ coherences. Thus, for sequential resonance assignments of fully protonated proteorhodopsin, we chose the combination of two strategies that leverage the longer lifetimes of the $^{13}C'$ spins by using *J*-mediated $^{13}C'$-$^{13}C\alpha$ coherence transfers[24] and detection of either H^{N}[5d] or Hα resonances.[11b] These two approaches, respectively, use (H)CANH and (H)(CO)CA(CO)NH spectra to correlate signals from $^{1}H-^{15}N$ amide pairs to $^{13}C\alpha$ resonances of adjacent residues, or use (H)NCAHA and (H)N(CO)CAHA to correlate the signals of $^{1}H\alpha-^{13}C\alpha$ pairs to intra and inter-residue ^{15}N species.[11b] Sequential backbone assignments are achieved by simultaneously linking correlations of both $^{1}H-^{15}N$ or $^{1}H\alpha-^{13}C\alpha$ pairs through their mutual $^{13}C\alpha$ or ^{15}N chemical shifts established in the amide or α proton-detected spectra, respectively, as depicted in Figure 3. Here,

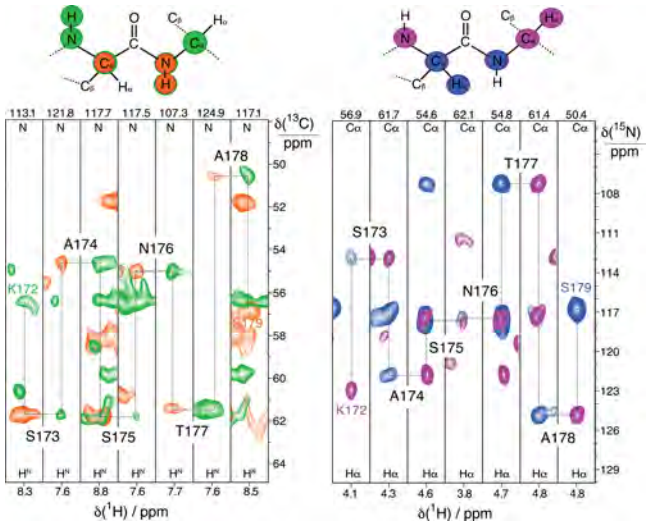

Figure 3. Sequential assignments of intensity correlations for residues 172−179 in fully protonated proteorhodopsin in lipids bilayers. 2D $^{1}H\alpha-^{13}C\alpha$ slices extracted from (H)CANH (green trace) and (H)(CO)CA(CO)NH (orange trace) spectra are shown in the left panel, and 2D $^{1}H-^{15}N$ slices from (H)NCAHA (magenta trace) and (H)N(CO)CAHA (blue trace) spectra in the right. The four spectra were acquired at 100 kHz MAS and 23.5 T.

representative portions of the four spectra that demonstrate sequential linking of amide and alpha pairs are reported. The choice of these pairs of experiments is motivated by the coherence lifetimes, which for membrane proteins are not as long as for microcrystalline samples. For comparison, while these 3D spectra were acquired in less than 2 weeks (Figure S1), $^{1}H^{N}$-detected experiments that rely on the faster decaying $^{13}C\alpha$ spins to enable $^{13}C'$- or $^{13}C\beta$-linking[25] have lower transfer efficiencies and significantly longer acquisition times. The $^{1}H\alpha-^{13}C\alpha$ and $^{1}H-^{15}N$ pairs also have roughly equal sensitivities, and the narrow dispersion in the $^{1}H\alpha$ dimension is offset by the narrow line width. This makes both types of spin pairs similarly useful in providing sequence-specific assignments. The backbone resonance assignments are further corroborated by analyses of the $^{13}C-^{13}C$-^{1}H TOCSY spectrum (Figure S4) that yields the assignment of the ^{1}H and ^{13}C side-chain resonances, thus enabling the identification of the amino acid types.

Resonance assignments for extensive portions of the proteorhodopsin backbone and side-chains were made based on spectra acquired at 100 kHz MAS. Despite the high degeneracy of aliphatic residues (32 Leu, 32 Ala, 24 Gly, 21 Val, and 19 Ile residues) that account for 49% of the proteorhodopsin sequence and the typically low chemical shift dispersions for helical proteins, the backbone resonances of 146 residues were sequence specifically assigned (Figure S5). Continuous linkages through 5 of the 6 proline residues were identified from analyses of $^{1}H\alpha$-detected 3D NMR correlation spectra. These residues are distributed in the transmembrane helices and extra-membrane loop regions. Importantly, resonance assignments were established for 57% of the ^{1}H and ^{13}C moieties of the aliphatic side-chains. The backbone chemical shifts clearly identify the seven transmembrane helices, connected by interhelical loops, and one additional short helix located in the extracellular E−F loop, in agreement with the structure of proteorhodopsin in detergents (Figure S6).

Such extensive resonance assignments facilitate the identification of inter-residue $^{1}H-^{1}H$ proximities that yield detailed site-specific information on proteorhodopsin structure in lipids. Key insights into the intra- and interhelical proximities between side-chains are obtained from analyses of high-resolution radio frequency-driven-recoupling (RFDR) spectra. For example, the 3D H(H)CH RFDR spectrum (1.4 ms mixing time, Figure 4) acquired from fully protonated proteorhodopsin shows numerous cross-signals that can be assigned to specific ^{1}H species using the resonance assignments established above. Subsequent analyses yield the identification of structural constraints, several of which are depicted schematically on the protein structure derived by solution NMR data, shown in Figure 4B. These include both intrahelical proximities, such as between the methyl ^{1}H of M134 and $^{1}H\alpha$ of G138 (Figure 4B, right, middle), and interhelical proximities, including the methyl ^{1}Hs of A116 and V182 (Figure 4B, right, bottom). These internuclear contacts within the transmembrane region are a direct way to probe the relative orientations of secondary structural elements. Especially important are the $^{1}H-^{1}H$ proximities of the $^{1}H\alpha$ of Gly residues and methyl groups, as these provide extremely useful structural constraints for α-helical proteins. In addition, the spectrum contains $^{1}H-^{1}H$ cross peaks between $^{1}H\alpha$ of Gly155 and two methyl groups with ^{1}H signals at 2.0 and 1.6 ppm, respectively, which are tentatively assigned to the retinal cofactor (Figure 4B, right, top). Such signals are valuable to establish the location, orientation and configuration of the chromophore in the transmembrane region of the protein, which is directly related to the protein functionality. In contrast, similar 3D spectra using perdeuterated and back-exchanged proteorhodopsin can only reveal $^{1}H^{N}-^{1}H^{N}$ contacts that primarily provide short- and medium-range intrahelical distance restraints. Importantly, much higher signal sensitivity and resolution were observed

DOI: 10.1021/jacs.7b05269
J. Am. Chem. Soc. 2017, 139, 13006−13012

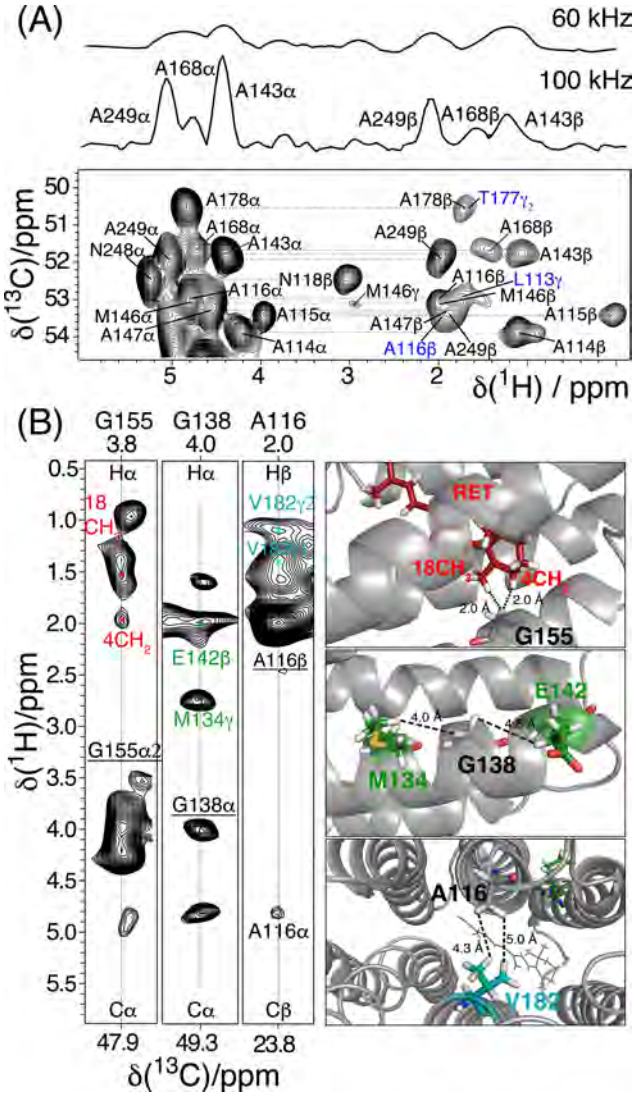

Figure 4. A) Alanine region of the 2D $^{1}H-^{13}C$ projection of a 3D H(H)CH RFDR spectrum acquired on U−[^{15}N,^{13}C] proteorhodopsin in lipids at 100 kHz MAS at 305 K and 23.5 T, using a 1.4 ms mixing time during which the RFDR rf-field was 200 kHz. Diagonal peaks are labeled in black and cross peaks in blue. Shown above the 2D projection are 1D ^{13}C slices extracted at the A249 Cα−Hα position (~51.9 ppm in the indirect dimension of the 2D projection) from the 3D RFDR spectrum acquired at 100 kHz and (up 60 kHz MAS. (B) 2D cross sections (left) of the 3D RFDR spectrum with $^{1}H-^{1}H$ correlations assigned to intra/interhelical and helix-retinal contacts cofactor, as depicted in the schematic 3D structure of the protein (right).

from the fully protonated sample at 100 kHz MAS versus an otherwise identical measurement at 60 kHz MAS on a 5-fold larger sample (Figure 4A).

The structures and properties of fully protonated membrane proteins in lipid bilayers are expected to closely resemble those in native cell-membrane environments. Interestingly, all of the $^{1}H-^{1}H$ contacts between the transmembrane helices reported above can be explained on the basis of the structure of proteorhodopsin in micellar (diheptanoyl-phosphocholine, diC$_7$PC) surfactant solution.[13] In combination with the ^{13}C chemical shift analysis above, this establishes that for the compositions and conditions investigated, the structures of proteorhodopsin in lipid bilayers and in micellar surfactant solution are very similar, and that even the position of the retinal cofactor within the transmembrane pocket is maintained. While in many cases solubilizing detergents have been observed to alter the structures or functionalities of membrane proteins,[26] that is not the case here. NMR structural analyses of fully protonated membrane proteins in lipids enabled by fast MAS represent an essential step to validating the conclusions from solution NMR data in detergent micelles.

From the present data, the oligomeric state of proteorhodopsin in lipid bilayers cannot be concluded, since it is not possible to identify any intermonomer cross peak in the 3D H(H)CH RFDR spectrum reflecting the presence of pentamers and/or hexamers. Unambiguous detection of such cross-peaks is extremely challenging due to the partial side chain assignment, the signal degeneracy, and the sample heterogeneity in terms of oligomeric composition. In order to identify such contacts, different strategies aimed at decreasing the sample heterogeneity and the spectral overlap and increasing the signal sensitivity can be adopted, such as the expression of mutants that stabilize a single oligomeric form to increase the sample homogeneity, or the use of tailored labeling schemes to decrease the spectral crowding, the acquisition of selective proton−proton distance restraints to increase the signal-to-noise, or the acquisition of 4D spectra with increased heteronuclear dimensionality to improve the spectral resolution.

CONCLUSIONS

Extensive atomic-level structural insights on a fully protonated membrane protein in native-like lipid environments are provided by ^{1}H-detected solid-state NMR spectra acquired under 100 kHz MAS conditions and at high (23.5 T) magnetic field. This approach yields highly resolved ^{1}H resonances from moieties throughout the protein, including those from transmembrane amide sites that are generally inaccessible to chemical exchange with water, and that are therefore absent in spectra of perdeuterated samples. This enables the sequential assignments of the protein resonances, including the majority of the aliphatic ^{1}H moieties, and notably the identification of long-range interhelical $^{1}H-^{1}H$ contacts between side-chains in transmembrane protein regions. To the best of our knowledge, this is the first report of long-range proximities between side-chain protons in a fully protonated membrane protein. Remarkably, this information was obtained with less than 0.5 mg of sample without the need for deuteration, thus circumventing a major roadblock to the structural characterization of membrane proteins by solid-state MAS NMR or other methods. This represents an important step toward the determination of membrane protein structures and their relationships to functional interactions in native-like lipid environments. The approach is expected to open opportunities to investigate a variety of complicated structure-dependent biochemical phenomena, including protein interactions in near-native environments or molecular recognition mechanisms that govern ligand binding to transmembrane receptors.

ASSOCIATED CONTENT

Supporting Information

The Supporting Information is available free of charge on the ACS Publications website at DOI: 10.1021/jacs.7b05269.

NMR coherence lifetimes and line widths. Diagrams with the NMR pulse sequence used. 2D $^{1}H-^{15}N$ CP−HSQC

DOI: 10.1021/jacs.7b05269
J. Am. Chem. Soc. 2017, 139, 13006−13012

NMR spectra acquired for U−[^{15}N, ^{13}C] PR in a 1.3 mm probe at 60 kHz and in a 0.7 mm probe at 100 kHz. ^{13}C−^{13}C 2D projection of the 3D (H)CCH-TOCSY spectrum. Topological plot of PR with the assigned residues and prediction of the secondary structure based on the analysis of the backbone chemical shifts. Probe considerations. Table of fully assigned ^{1}H, ^{13}C, and ^{15}N chemical shifts (PDF)

AUTHOR INFORMATION

Corresponding Authors

*bradc@engineering.ucsb.edu

*guido.pintacuda@ens-lyon.fr

ORCID

Bradley F. Chmelka: 0000-0002-4450-6949

Guido Pintacuda: 0000-0001-7757-2144

Present Address

‖Max-Plank Institute for Biophysical Chemistry, Am Fassberg 11, Göttingen, Germany.

Notes

The authors declare no competing financial interest.

ACKNOWLEDGMENTS

Financial support is acknowledged from the French CNRS (IR-RMN FR3050), from the European Research Council (ERC) under the European Union's Horizon 2020 Research and Innovation Programme (ERC-2015-CoG GA no. 648974), from the National Institutes of Health (R01GM116128), and from the USARO through the Institute for Collaborative Biotechnologies (grant W911NF-09-0001) and award W911NF-14-1-0617. L.B.A was supported by a MC incoming fellowships (REA grant agreement no. 624918 "MEM-MAS").

REFERENCES

(1) (a) Lange, A.; Giller, K.; Hornig, S.; Martin-Eauclaire, M. F.; Pongs, O.; Becker, S.; Baldus, M. *Nature* **2006**, *440*, 959−962. (b) Xu, J.; Durr, U. H.; Im, S. C.; Gan, Z.; Waskell, L.; Ramamoorthy, A. *Angew. Chem., Int. Ed.* **2008**, *47*, 7864−7867. (c) Etzkorn, M.; Kneuper, H.; Dunnwald, P.; Vijayan, V.; Kramer, J.; Griesinger, C.; Becker, S.; Unden, G.; Baldus, M. *Nat. Struct. Mol. Biol.* **2008**, *15*, 1031−1039. (d) Bajaj, V. S.; Mak-Jurkauskas, M. L.; Belenky, M.; Herzfeld, J.; Griffin, R. G. *Proc. Natl. Acad. Sci. U. S. A.* **2009**, *106*, 9244−9249. (e) Cady, S. D.; Schmidt-Rohr, K.; Wang, J.; Soto, C. S.; Degrado, W. F.; Hong, M. *Nature* **2010**, *463*, 689−692. (f) Sharma, M.; Yi, M.; Dong, H.; Qin, H.; Peterson, E.; Busath, D. D.; Zhou, H. X.; Cross, T. A. *Science* **2010**, *330*, 509−512. (g) Bhate, M. P.; McDermott, A. E. *Proc. Natl. Acad. Sci. U. S. A.* **2012**, *109*, 15265−15270. (h) Park, S. H.; Das, B. B.; Casagrande, F.; Tian, Y.; Nothnagel, H. J.; Chu, M.; Kiefer, H.; Maier, K.; De Angelis, A. A.; Marassi, F. M.; Opella, S. J. *Nature* **2012**, *491*, 779−783. (i) Shahid, S. A.; Bardiaux, B.; Franks, W. T.; Krabben, L.; Habeck, M.; van Rossum, B. J.; Linke, D. *Nat. Methods* **2012**, *9*, 1212−1217. (j) Wang, S.; Munro, R. A.; Shi, L.; Kawamura, I.; Okitsu, T.; Wada, A.; Kim, S. Y.; Jung, K. H.; Brown, L. S.; Ladizhansky, V. *Nat. Methods* **2013**, *10*, 1007−1012. (k) Wylie, B. J.; Bhate, M. P.; McDermott, A. E. *Proc. Natl. Acad. Sci. U. S. A.* **2014**, *111*, 185−190. (l) Andreas, L. B.; Reese, M.; Eddy, M. T.; Gelev, V.; Ni, Q. Z.; Miller, E. A.; Emsley, L.; Pintacuda, G.; Chou, J. J.; Griffin, R. G. *J. Am. Chem. Soc.* **2015**, *137*, 14877−14886. (m) Becker-Baldus, J.; Bamann, C.; Saxena, K.; Gustmann, H.; Brown, L. J.; Brown, R. C.; Reiter, C.; Bamberg, E.; Wachtveitl, J.; Schwalbe, H.; Glaubitz, C. *Proc. Natl. Acad. Sci. U. S. A.* **2015**, *112*, 9896−9901.

(2) Andreas, L. B.; Le Marchand, T.; Jaudzems, K.; Pintacuda, G. *J. Magn. Reson.* **2015**, *253*, 36−49.

(3) (a) Samoson, A.; Tuherm, T.; Gan, Z. *Solid State Nucl. Magn. Reson.* **2001**, *20*, 130−136. (b) Zhou, D. H.; Shea, J. J.; Nieuwkoop, A. J.; Franks, W. T.; Wylie, B. J.; Mullen, C.; Sandoz, D.; Rienstra, C. M. *Angew. Chem., Int. Ed.* **2007**, *46*, 8380−8383. (c) Marchetti, A.; Jehle, S.; Felletti, M.; Knight, M. J.; Wang, Y.; Xu, Z. Q.; Park, A. Y.; Otting, G.; Lesage, A.; Emsley, L.; Dixon, N. E.; Pintacuda, G. *Angew. Chem., Int. Ed.* **2012**, *51*, 10756−10759. (d) Vasa, S. K.; Rovo, P.; Giller, K.; Becker, S.; Linser, R. *Phys. Chem. Chem. Phys.* **2016**, *18*, 8359−8363.

(4) (a) Paulson, E. K.; Morcombe, C. R.; Gaponenko, V.; Dancheck, B.; Byrd, R. A.; Zilm, K. W. *J. Am. Chem. Soc.* **2003**, *125*, 15831−15836. (b) Chevelkov, V.; Rehbein, K.; Diehl, A.; Reif, B. *Angew. Chem., Int. Ed.* **2006**, *45*, 3878−3881.

(5) (a) Zhou, D. H.; Shah, G.; Cormos, M.; Mullen, C.; Sandoz, D.; Rienstra, C. M. *J. Am. Chem. Soc.* **2007**, *129*, 11791−11801. (b) Knight, M. J.; Webber, A. L.; Pell, A. J.; Guerry, P.; Barbet-Massin, E.; Bertini, I.; Felli, I. C.; Gonnelli, L.; Pierattelli, R.; Emsley, L.; Lesage, A.; Herrmann, T.; Pintacuda, G. *Angew. Chem., Int. Ed.* **2011**, *50*, 11697−11701. (c) Knight, M. J.; Pell, A. J.; Bertini, I.; Felli, I. C.; Gonnelli, L.; Pierattelli, R.; Herrmann, T.; Emsley, L.; Pintacuda, G. *Proc. Natl. Acad. Sci. U. S. A.* **2012**, *109*, 11095−11100. (d) Barbet-Massin, E.; Pell, A. J.; Retel, J. S.; Andreas, L. B.; Jaudzems, K.; Franks, W. T.; Nieuwkoop, A. J.; Hiller, M.; Higman, V.; Guerry, P.; Bertarello, A.; Knight, M. J.; Felletti, M.; Le Marchand, T.; Kotelovica, S.; Akopjana, I.; Tars, K.; Stoppini, M.; Bellotti, V.; Bolognesi, M.; Ricagno, S.; Chou, J. J.; Griffin, R. G.; Oschkinat, H.; Lesage, A.; Emsley, L.; Herrmann, T.; Pintacuda, G. *J. Am. Chem. Soc.* **2014**, *136*, 12489−12497. (e) Lamley, J. M.; Iuga, D.; Oster, C.; Sass, H. J.; Rogowski, M.; Oss, A.; Past, J.; Reinhold, A.; Grzesiek, S.; Samoson, A.; Lewandowski, J. R. *J. Am. Chem. Soc.* **2014**, *136*, 16800−16806. (f) Agarwal, V.; Penzel, S.; Szekely, K.; Cadalbert, R.; Testori, E.; Oss, A.; Past, J.; Samoson, A.; Ernst, M.; Bockmann, A.; Meier, B. H. *Angew. Chem., Int. Ed.* **2014**, *53*, 12253−12256. (g) Sinnige, T.; Daniels, M.; Baldus, M.; Weingarth, M. *J. Am. Chem. Soc.* **2014**, *136*, 4452−4455. (h) Mance, D.; Sinnige, T.; Kaplan, M.; Narasimhan, S.; Daniels, M.; Houben, K.; Baldus, M.; Weingarth, M. *Angew. Chem., Int. Ed.* **2015**, *54*, 15799−15803.

(6) Ward, M. E.; Shi, L.; Lake, E.; Krishnamurthy, S.; Hutchins, H.; Brown, L. S.; Ladizhansky, V. *J. Am. Chem. Soc.* **2011**, *133*, 17434−17443.

(7) (a) Zhou, D. H.; Nieuwkoop, A. J.; Berthold, D. A.; Comellas, G.; Sperling, L. J.; Tang, M.; Shah, G. J.; Brea, E. J.; Lemkau, L. R.; Rienstra, C. M. *J. Biomol. NMR* **2012**, *54*, 291−305. (b) Eddy, M. T.; Su, Y.; Silvers, R.; Andreas, L.; Clark, L.; Wagner, G.; Pintacuda, G.; Emsley, L.; Griffin, R. G. *J. Biomol. NMR* **2015**, *61*, 299−310.

(8) Medeiros-Silva, J.; Mance, D.; Daniels, M.; Jekhmane, S.; Houben, K.; Baldus, M.; Weingarth, M. *Angew. Chem., Int. Ed.* **2016**, *55*, 13606−13610.

(9) Nishiyama, Y. *Solid State Nucl. Magn. Reson.* **2016**, *78*, 24−36.

(10) Andreas, L. B.; Jaudzems, K.; Stanek, J.; Lalli, D.; Bertarello, A.; Le Marchand, T.; Cala-De Paepe, D.; Kotelovica, S.; Akopjana, I.; Knott, B.; Wegner, S.; Engelke, F.; Lesage, A.; Emsley, L.; Tars, K.; Herrmann, T.; Pintacuda, G. *Proc. Natl. Acad. Sci. U. S. A.* **2016**, *113*, 9187−9192.

(11) (a) Mroue, K. H.; Nishiyama, Y.; Kumar Pandey, M.; Gong, B.; McNerny, E.; Kohn, D. H.; Morris, M. D.; Ramamoorthy, A. *Sci. Rep.* **2015**, *5*, 11991. (b) Stanek, J.; Andreas, L. B.; Jaudzems, K.; Cala, D.; Lalli, D.; Bertarello, A.; Schubeis, T.; Akopjana, I.; Kotelovica, S.; Tars, K.; Pica, A.; Leone, S.; Picone, D.; Xu, Z. Q.; Dixon, N. E.; Martinez, D.; Berbon, M.; El Mammeri, N.; Noubhani, A.; Saupe, S.; Habenstein, B.; Loquet, A.; Pintacuda, G. *Angew. Chem., Int. Ed.* **2016**, *55*, 15504−15509.

(12) (a) Bamann, C.; Bamberg, E.; Wachtveitl, J.; Glaubitz, C. *Biochim. Biophys. Acta, Bioenerg.* **2014**, *1837*, 614−625. (b) Inoue, K.; Kato, Y.; Kandori, H. *Trends Microbiol.* **2015**, *23*, 91−98.

(13) Reckel, S.; Gottstein, D.; Stehle, J.; Lohr, F.; Verhoefen, M. K.; Takeda, M.; Silvers, R.; Kainosho, M.; Glaubitz, C.; Wachtveitl, J.; Bernhard, F.; Schwalbe, H.; Guntert, P.; Dotsch, V. *Angew. Chem., Int. Ed.* **2011**, *50*, 11942−11946.

DOI: 10.1021/jacs.7b05269
J. Am. Chem. Soc. 2017, 139, 13006−13012

(14) (a) Stone, K. M.; Voska, J.; Kinnebrew, M.; Pavlova, A.; Junk, M. J.; Han, S. *Biophys. J.* **2013**, *104*, 472−481. (b) Edwards, D. T.; Huber, T.; Hussain, S.; Stone, K. M.; Kinnebrew, M.; Kaminker, I.; Matalon, E.; Sherwin, M. S.; Goldfarb, D.; Han, S. *Structure* **2014**, *22*, 1677−1686. (c) Maciejko, J.; Mehler, M.; Kaur, J.; Lieblein, T.; Morgner, N.; Ouari, O.; Tordo, P.; Becker-Baldus, J.; Glaubitz, C. *J. Am. Chem. Soc.* **2015**, *137*, 9032−9043.
(15) (a) Shi, L.; Ahmed, M. A. M.; Zhang, W.; Whited, G.; Brown, L. S.; Ladizhansky, V. *J. Mol. Biol.* **2009**, *386*, 1078−1093. (b) Shi, L.; Lake, E. M.; Ahmed, M. A.; Brown, L. S.; Ladizhansky, V. *Biochim. Biophys. Acta, Biomembr.* **2009**, *1788*, 2563−2574.
(16) Bennett, A. E.; Rienstra, C. M.; Auger, M.; Lakshmi, K. V.; Griffin, R. G. *J. Chem. Phys.* **1995**, *103*, 6951−6958.
(17) Zhou, D. H.; Rienstra, C. M. *J. Magn. Reson.* **2008**, *192*, 167−172.
(18) (a) Good, D. B.; Wang, S.; Ward, M. E.; Struppe, J.; Brown, L. S.; Lewandowski, J. R.; Ladizhansky, V. *J. Am. Chem. Soc.* **2014**, *136*, 2833−2842. (b) Saurel, O.; Iordanov, I.; Nars, G.; Demange, P.; Le Marchand, T.; Andreas, L. B.; Pintacuda, G.; Milon, A. *J. Am. Chem. Soc.* **2017**, *139*, 1590−1597.
(19) Asami, S.; Szekely, K.; Schanda, P.; Meier, B. H.; Reif, B. *J. Biomol. NMR* **2012**, *54*, 155−168.
(20) Asami, S.; Schmieder, P.; Reif, B. *J. Am. Chem. Soc.* **2010**, *132*, 15133−15135.
(21) Huber, M.; Hiller, S.; Schanda, P.; Ernst, M.; Bockmann, A.; Verel, R.; Meier, B. H. *ChemPhysChem* **2011**, *12*, 915−918.
(22) Wang, S.; Parthasarathy, S.; Nishiyama, Y.; Endo, Y.; Nemoto, T.; Yamauchi, K.; Asakura, T.; Takeda, M.; Terauchi, T.; Kainosho, M.; Ishii, Y. *PLoS One* **2015**, *10*, e0122714.
(23) (a) Venters, R. A.; Farmer, B. T., II; Fierke, C. A.; Spicer, L. D. *J. Mol. Biol.* **1996**, *264*, 1101−1116. (b) Smith, A. A.; Ravotti, F.; Testori, E.; Cadalbert, R.; Ernst, M.; Bockmann, A.; Meier, B. H. *J. Biomol. NMR* **2017**, *67*, 109−119.
(24) Barbet-Massin, E.; Pell, A. J.; Jaudzems, K.; Franks, W. T.; Retel, J. S.; Kotelovica, S.; Akopjana, I.; Tars, K.; Emsley, L.; Oschkinat, H.; Lesage, A.; Pintacuda, G. *J. Biomol. NMR* **2013**, *56*, 379−386.
(25) Barbet-Massin, E.; Pell, A. J.; Knight, M. J.; Webber, A. L.; Felli, I. C.; Pierattelli, R.; Emsley, L.; Lesage, A.; Pintacuda, G. *ChemPhysChem* **2013**, *14*, 3131−3137.
(26) Cross, T. A.; Sharma, M.; Yi, M.; Zhou, H. X. *Trends Biochem. Sci.* **2011**, *36*, 117−125.

DOI: 10.1021/jacs.7b05269
J. Am. Chem. Soc. 2017, 139, 13006−13012

SUPPORTING INFORMATION

Proton-based structural analysis of a heptahelical transmembrane protein in lipid bilayers

Daniela Lalli,[a] Matthew N. Idso,[b] Loren B. Andreas,[a],† Sunyia Hussain,[b] Naomi Baxter, [c] Songi Han,[b,c] Bradley F. Chmelka,[b]* and Guido Pintacuda[a]*

[a] Centre de RMN à Très Hauts Champs, Institut des Sciences Analytiques (UMR 5280-CNRS, ENS Lyon, UCB Lyon 1), Université de Lyon, 69100 Villeurbanne, France

[b] Department of Chemical Engineering, University of California, Santa Barbara, California, 93106 United States

[c] Department of Chemistry and Biochemistry, University of California, Santa Barbara, California, 93106 United States

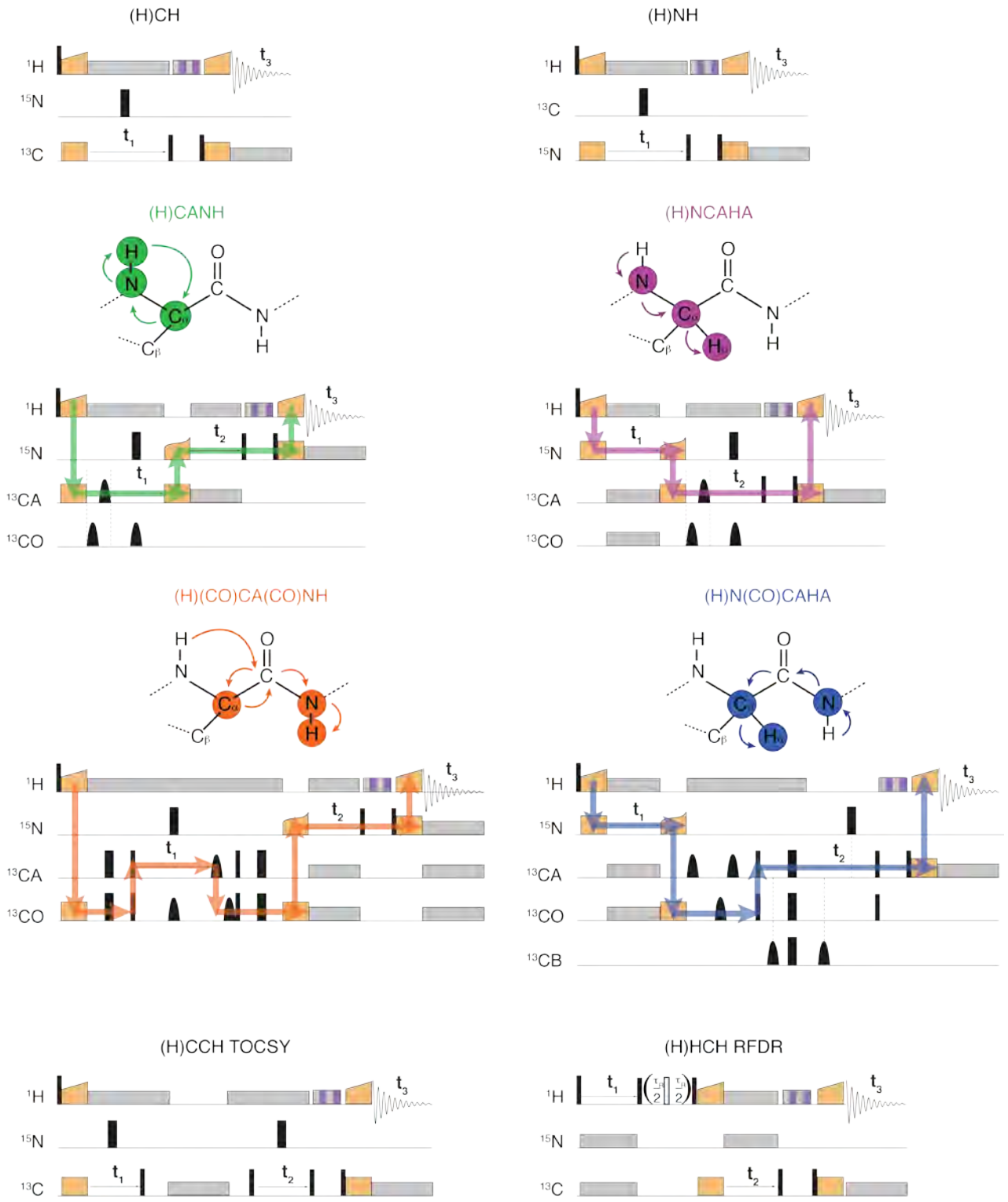

Figure S1: Pulse sequence schemes for all of the experiments acquired on proteorhodopsin samples and presented in the main text. Narrow and broad black rectangles indicate π/2 and π pulses, respectively, and bell shapes represent band-selective inversion pulses. For the H^N-detected correlation experiments (H)CANH and (H)(CO)CA(CO)NH,[1] and for the H detected experiments (H)NCAHA and (H)N(CO)CAHA,[2] the coherence pathways and chemical shift evolution of ^{13}C and ^{15}N nuclei are shown as arrows colored in green, orange, magenta and blue, respectively.

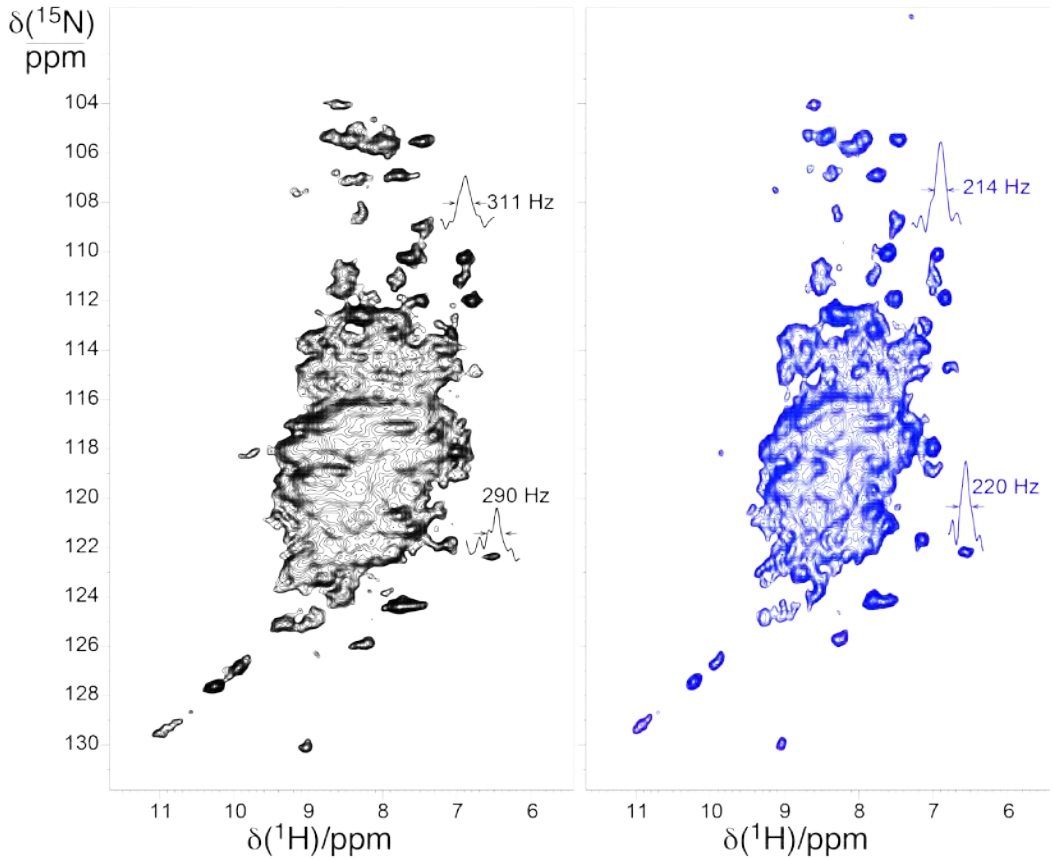

Figure S2. 2D ^{1}H-^{15}N CP-HSQC NMR spectra acquired for U-[^{15}N, ^{13}C] proteorhodopsin in a 1.3 mm probe at 60 kHz (black) and in a 0.7 mm probe at 100 kHz (blue).

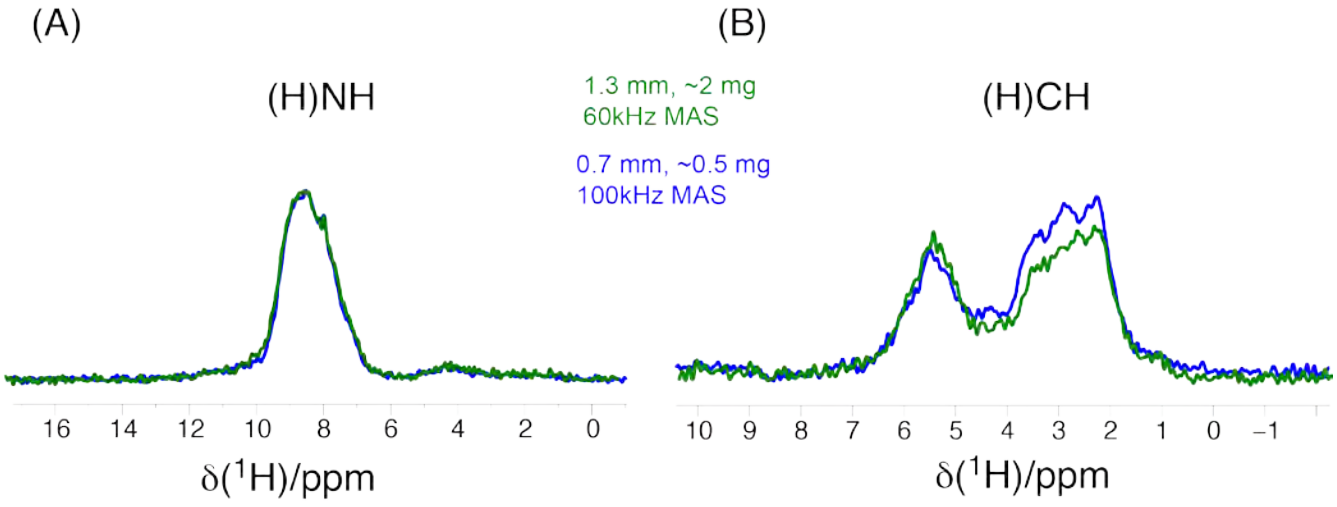

Figure S3. Comparison of optimized (H)NH and (H)CH spectra of U-[^{15}N, ^{13}C] proteorhodopsin acquired (A) in a 1.3 mm probe at 60 kHz (green) and (B) in the 0.7 mm probe at 100 kHz (blue). Both spectra were recorded with the same number of scans at 1 GHz, and no line broadening was applied.

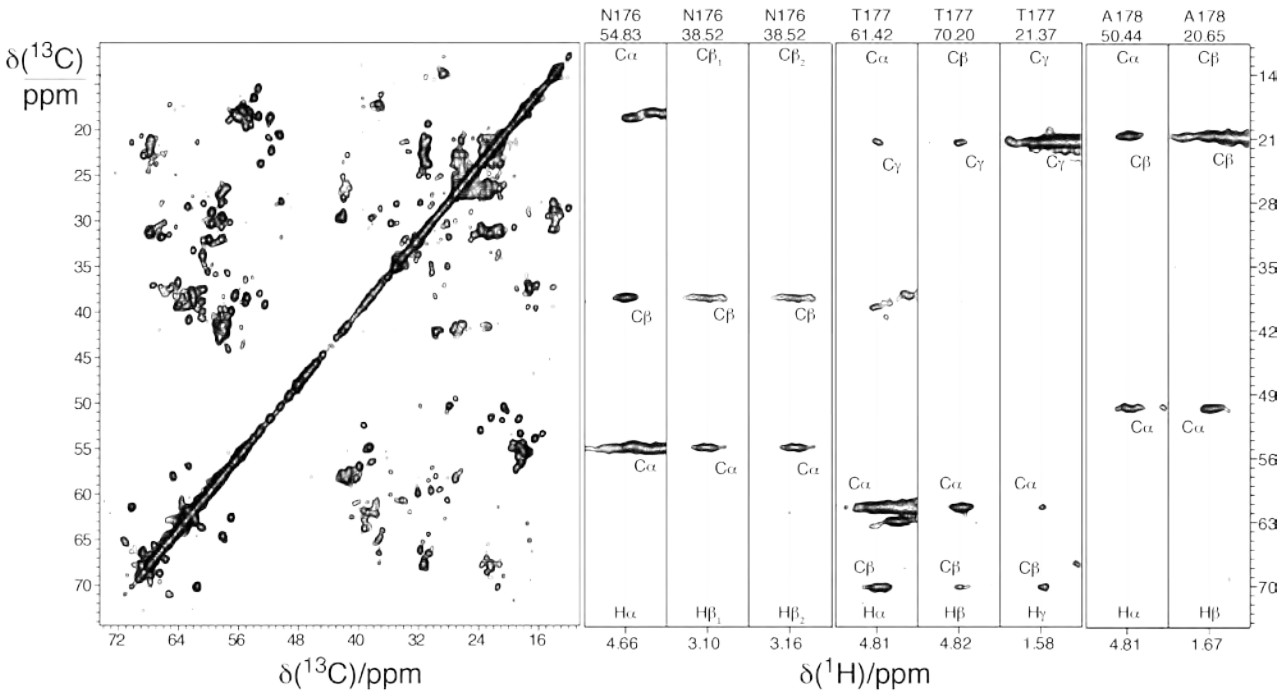

Figure S4: ^{13}C-^{13}C 2D projection of the 3D hCCH-TOCSY spectrum acquired on ^{15}N, ^{13}C proteorhodopsin in lipid bilayers, at the 1 GHz spinning at 100 kHz MAS, in a 0.7 mm probe. WALTZ-16 at 25 kHz was applied for the TOCSY mixing of 15 ms. Examples of carbon and proton side chain assignments are reported for residues 176-178 through strips extracted from the 3D ^{13}C-^{13}C-TOCSY spectrum.

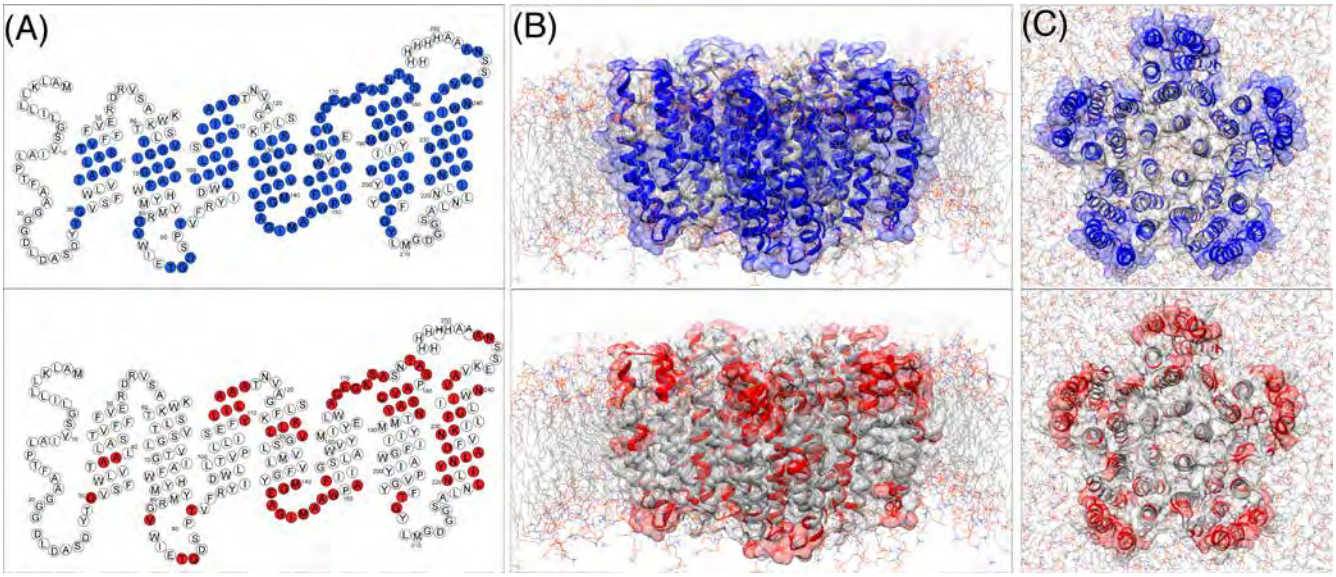

Figure S5. (A) Topological plot of proteorhodopsin, where the assigned residues are highlighted in blue for the U-[^{15}N, ^{13}C] sample and in red for the U-[^{2}H,^{15}N,^{13}C] 100% back-exchanged one. The assigned residues are reported on the PR structure with the same color code and shown in panels (B) and (C). PR monomers (pdb code: 2L6X) are modeled into pentamers by using the multi-docking High Ambiguity-Driven DOCKing (HADDOCK)[3] program and shown embedded into lipid bilayers with horizontal (B) and axial (C) orientations.

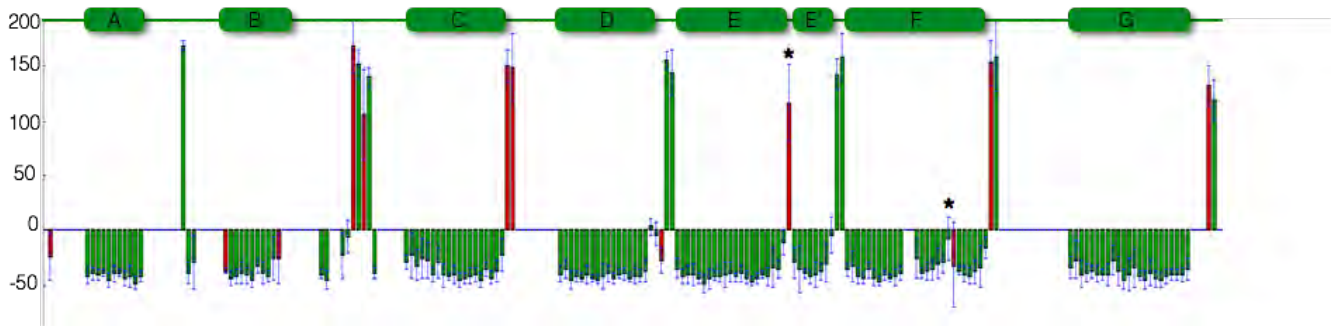

Figure S6. Prediction of the secondary structure performed by TALOS+ based on the analysis of the proteorhodopsin backbone chemical shifts (N, H^N, C', Cα, Cβ). The predicted average backbone torsion angle ψ is reported as a function of the protein sequence (the green boxes represent helices A-G and the lines depict the loops). Negative ψ values indicate helical structure, while positive ψ values beta strands or deviations from helicity. Distortion in helices E at position G169 and F at position V200, P201 are indicated with an asterisk. Overall these structural features are preserved in micelles.

Table S1. ^{13}C', ^{13}CA, ^{15}N and $^{1}H^N$ coherence lifetimes measured at 60 kHz and 100 kHz MAS, at the 1 GHz, via a ^{1}H-^{13}C CP sequence with a selective echo (for carbon T_2') or by using a standard Hahn echo sequence (for proton and nitrogen T_2'). During ^{13}C, ^{15}N chemical shift evolution, swept low-power TPPM (slTPPM)[4] was used on ^{1}H with a RF frequency of 25 kHz.

	^{1}H		^{15}N		^{13}C'		^{13}Cα	
MAS rate	60 kHz	100 kHz	60 kHz	100 kHz	60 kHz	100 kHz	60 kHz	100 kHz
Bulk T2'	1.3 ms	2.5 ms	18 ms	21 ms	18.5 ms	21 ms	9 ms	12.5 ms

Table S2. Acquisition and processing parameters for the NMR experiments acquired on the U-[^{15}N,^{13}C] proteorhodopsin, at the 1 GHz in a 0.7 mm probe, spinning at 100 kHz. The direct proton dimension was sampled to 10 ms.

Spectrum	Max indirect evolution	Scans per point	Experimental time	Signal/Noise (First FID)	Processing
(H)NH[a]	20.4 ms (N)	64	2.5 h	131	60-deg shifted sine-bell squared
(H)NH	31.5 ms (N)	128	9 h	120	60-deg shifted sine-bell squared
(H)CH	13 ms (C)	32	4.5 h	87	60-deg shifted sine-bell squared
(H)NCAH	5 ms (CA), 8 ms (N)	16	18 h	25	90-deg shifted sine-bell squared
(H)N(CO)CAH	5 ms (CA), 8 ms (N)	32	44.5 h	13	90-deg shifted sine-bell squared
(H)CANH	6 ms (CA), 9.2 ms (N)	24	33 h	18	90-deg shifted sine-bell squared
(H)(CO)CA(CO)NH	6 ms (CA), 9.2 ms (N)	32	45 h	11	90-deg shifted sine-bell squared
(H)CONH	11 ms (C'), 9.2 ms (N)	16	22.5 h	16	90-deg shifted sine-bell squared
(H)CCH-TOCSY (15 ms)	6.5 ms	12	147 h	32	90-deg shifted sine-bell squared
(H)HCH-RFDR (1.4 ms)	5.3 ms (H), 6.5 ms (C)	16	117 h	92	90-deg shifted sine-bell squared

[a] Acquisition and processing parameters for the (H)NH experiments acquired on the U-[^{2}H,^{15}N,^{13}C] PR 100% back-exchanged spinning at 60 kHz in a 1.3 mm probe. The direct proton dimension was sampled to 12.5 ms.

Table S3. Assignment of backbone and side chains resonances of ^{13}C ^{15}N proteorhodopsin in lipid bilayers, referenced to adamantane (^{1}H signal at 1.87 ppm).

a.a.			(ppm)	a.a.			(ppm)	a.a.			(ppm)
THR	29	C	176.3	VAL	129	C	177.8	PRO	180	C	179.3
THR	29	CA	64.7	VAL	129	CA	67.6	PRO	180	CA	66.1
THR	29	N	107.1	VAL	129	CB	31.2	PRO	180	CB	31.7
THR	29	H	7.6	VAL	129	CG1	23.6	PRO	180	CD	50.3
GLY	30	CA	45.9	VAL	129	CG2	22.4	PRO	180	CG	27.9
GLY	30	N	109.5	VAL	129	N	116.8	PRO	180	N	135.0
GLY	30	H	8.3	VAL	129	H	8.3	PRO	180	HG2	2.6
GLY	30	HA2	4.0	VAL	129	HA	3.7	PRO	180	HD	4.2
GLY	30	HA3	4.2	VAL	129	HB	2.4	PRO	180	HA	4.5
THR	37	C	175.7	VAL	129	HG1	1.3	PRO	180	HG3	2.3
THR	37	CA	69.2	VAL	129	HG2	1.1	PRO	180	HB2	2.1
THR	37	CB	68.5	GLY	130	C	175.7	PRO	180	HB3	2.7
THR	37	CG2	22.4	GLY	130	CA	47.9	ALA	181	C	180.7
THR	37	N	117.6	GLY	130	N	105.7	ALA	181	CA	55.2
THR	37	H	8.2	GLY	130	H	8.7	ALA	181	CB	18.1
THR	37	HA	4.7	GLY	130	HA3	4.0	ALA	181	N	119.4
THR	37	HB	4.4	GLY	130	HA2	4.1	ALA	181	H	8.6

THR	37	HG2	1.5	SER	131	C	175.5	ALA	181	HA	4.4
ALA	38	C	178.7	SER	131	CA	63.3	ALA	181	HB	1.7
ALA	38	CA	55.1	SER	131	CB	62.7	VAL	182	C	177.3
ALA	38	CB	18.4	SER	131	N	118.3	VAL	182	CA	66.7
ALA	38	N	121.2	SER	131	H	8.5	VAL	182	CB	30.7
ALA	38	HA	4.0	SER	131	HA	4.4	VAL	182	CG1	23.8
ALA	38	H	7.2	SER	131	HB	4.1	VAL	182	CG2	21.1
ALA	38	HB	1.7	LEU	132	C	178.8	VAL	182	N	121.2
ALA	39	C	180.6	LEU	132	CA	57.8	VAL	182	H	7.7
ALA	39	CA	55.0	LEU	132	CB	42.0	VAL	182	HA	3.9
ALA	39	CB	19.6	LEU	132	CD1	25.9	VAL	182	HB	2.5
ALA	39	N	119.0	LEU	132	CD2	22.7	VAL	182	HG1	1.4
ALA	39	H	8.3	LEU	132	CG	26.7	VAL	182	HG2	1.1
ALA	39	HA	4.2	LEU	132	N	122.5	GLN	183	C	178.5
ALA	39	HB	1.6	LEU	132	H	7.9	GLN	183	CA	60.6
LEU	40	C	180.2	LEU	132	HA	4.4	GLN	183	CB	28.1
LEU	40	CA	57.8	LEU	132	HB	1.6	GLN	183	CD	180.5
LEU	40	CB	42.0	LEU	132	HD2	1.1	GLN	183	CG	34.9
LEU	40	N	120.3	LEU	132	HG	2.3	GLN	183	N	119.9
LEU	40	H	8.9	LEU	132	HD1	1.1	GLN	183	NE2	112.3
LEU	40	HA	4.4	VAL	133	CA	67.9	GLN	183	H	8.9
LEU	40	CG	26.5	VAL	133	CB	31.4	GLN	183	HA	4.1
LEU	40	HB	1.5	VAL	133	CG1	23.7	GLN	183	HB	2.3
LEU	40	HG	1.1	VAL	133	CG2	22.5	GLN	183	HG	2.6
LEU	41	C	176.7	VAL	133	N	119.5	GLN	183	HE22	6.7
LEU	41	CA	58.5	VAL	133	H	8.7	GLN	183	HE21	7.4
LEU	41	CB	39.6	VAL	133	HA	3.8	SER	184	C	177.2
LEU	41	CG	25.7	VAL	133	HB	2.4	SER	184	CA	61.7
LEU	41	HA	3.5	VAL	133	HG2	1.1	SER	184	CB	62.9
LEU	41	N	124.9	VAL	133	HG1	1.3	SER	184	N	112.9
LEU	41	H	8.2	MET	134	C	176.7	SER	184	H	8.3
LEU	41	HB	1.6	MET	134	CA	59.5	SER	184	HA	4.6
ALA	42	C	178.8	MET	134	CB	34.8	SER	184	HB	4.3
ALA	42	CA	54.8	MET	134	CG	30.3	ALA	185	C	177.3
ALA	42	CB	18.5	MET	134	N	117.7	ALA	185	CA	55.5
ALA	42	N	117.9	MET	134	H	8.1	ALA	185	CB	17.9
ALA	42	H	7.8	MET	134	HA	4.4	ALA	185	N	124.9
ALA	42	HA	4.2	MET	134	HB	2.4	ALA	185	H	7.7
ALA	42	HB	1.8	MET	134	HG	2.6	ALA	185	HA	4.3
SER	43	C	173.2	LEU	135	C	178.9	ALA	185	HB	1.7
SER	43	CA	62.3	LEU	135	CA	57.3	TYR	186	C	177.7
SER	43	CB	62.4	LEU	135	CB	41.1	TYR	186	CA	61.9
SER	43	N	111.9	LEU	135	CD1	26.2	TYR	186	CB	38.8
SER	43	H	8.5	LEU	135	CD2	23.9	TYR	186	N	118.6
SER	43	HA	3.9	LEU	135	CG	26.4	TYR	186	H	9.1
SER	43	HB	3.9	LEU	135	N	113.5	TYR	186	HA	4.4
THR	44	CA	67.9	LEU	135	H	7.7	TYR	186	HB	3.2
THR	44	CB	68.9	LEU	135	HA	4.5	ASN	187	CA	56.4
THR	44	CG2	20.7	LEU	135	HB	2.4	ASN	187	CB	38.2
THR	44	N	118.8	LEU	135	HG	1.0	ASN	187	CG	175.6
THR	44	H	7.7	VAL	136	C	178.1	ASN	187	N	117.5
THR	44	HA	4.1	VAL	136	CA	67.5	ASN	187	H	8.7
THR	44	HB	4.6	VAL	136	CB	31.3	ASN	187	HA	4.6
THR	44	HG2	1.5	VAL	136	CG1	23.7	ASN	187	HB2	2.9
VAL	45	CA	67.6	VAL	136	CG2	22.3	ASN	187	HB3	3.3
VAL	45	CB	31.4	VAL	136	N	118.2	THR	188	C	176.5

VAL	45	CG2	21.1	VAL	136	H	9.0	THR	188	CA	68.1
VAL	45	N	118.3	VAL	136	HA	3.8	THR	188	CG2	22.5
VAL	45	H	7.4	VAL	136	HG1	1.3	THR	188	N	116.6
VAL	45	HA	3.7	VAL	136	HG2	1.1	THR	188	H	8.6
VAL	45	HB	2.3	VAL	136	HB	2.4	THR	188	HG2	1.6
VAL	45	HG2	1.2	PHE	137	C	177.8	THR	188	CB	67.8
VAL	45	CG1	22.4	PHE	137	CA	64.1	THR	188	HA	4.5
VAL	45	HG1	1.1	PHE	137	CB	36.8	MET	189	C	178.6
THR	63	CA	62.7	PHE	137	CG	144.0	MET	189	CA	60.1
THR	63	CB	64.0	PHE	137	N	117.0	MET	189	CB	35.6
THR	63	CG2	22.6	PHE	137	H	8.2	MET	189	CE	20.0
THR	63	HB	4.1	PHE	137	HA	4.3	MET	189	CG	30.2
THR	63	HA	4.4	PHE	137	HB	3.1	MET	189	N	120.2
THR	63	HG2	1.4	GLY	138	C	175.3	MET	189	H	9.0
VAL	64	CA	68.2	GLY	138	CA	49.4	MET	189	HA	4.0
VAL	64	CB	31.3	GLY	138	N	106.4	MET	189	HB	2.3
VAL	64	N	124.0	GLY	138	H	8.2	MET	189	HG	2.4
VAL	64	H	8.8	GLY	138	HA	4.0	MET	190	CA	59.8
VAL	64	HA	3.9	TYR	139	C	176.6	MET	190	CB	32.4
VAL	64	HB	2.4	TYR	139	CA	62.6	MET	190	CG	30.7
VAL	64	CG2	22.2	TYR	139	CB	39.2	MET	190	N	120.3
VAL	64	CG1	22.7	TYR	139	N	121.9	MET	190	HB	1.9
VAL	64	HG1	1.0	TYR	139	H	8.1	MET	190	HG	2.1
VAL	64	HG2	1.1	TYR	139	HA	3.8	MET	190	HA	4.1
SER	65	C	176.1	TYR	139	HB	3.1	MET	190	H	8.8
SER	65	CA	63.1	MET	140	C	179.3	ILE	194	C	174.4
SER	65	CB	62.4	MET	140	CA	60.7	ILE	194	CA	64.2
SER	65	N	116.6	MET	140	CB	34.2	ILE	194	CB	39.5
SER	65	H	7.4	MET	140	CG	32.3	ILE	194	CD1	14.2
SER	65	HA	4.4	MET	140	N	115.0	ILE	194	CG1	28.0
SER	65	HB	4.0	MET	140	H	8.3	ILE	194	CG2	16.5
GLY	66	C	175.9	MET	140	HA	3.7	ILE	194	N	117.4
GLY	66	CA	47.2	MET	140	HG	2.5	ILE	194	H	7.7
GLY	66	N	105.7	MET	140	HB	2.5	ILE	194	HD1	0.7
GLY	66	H	8.0	GLY	141	C	176.1	ILE	194	HB	1.6
GLY	66	HA2	4.7	GLY	141	CA	46.4	ILE	194	HA	4.2
GLY	66	HA3	4.5	GLY	141	N	107.4	ILE	194	HG2	0.2
		L67		GLY	141	H	8.3	ILE	194	HG1	2.0
VAL	68	C	177.7	GLY	141	HA	4.6	PHE	195	C	177.2
VAL	68	CA	67.6	GLU	142	C	178.3	PHE	195	CA	61.1
VAL	68	CB	31.3	GLU	142	CA	61.0	PHE	195	CB	40.5
VAL	68	CG1	23.6	GLU	142	CB	29.4	PHE	195	CD1	131.9
VAL	68	CG2	21.5	GLU	142	CD	179.0	PHE	195	CG	141.1
VAL	68	N	118.7	GLU	142	CG	32.5	PHE	195	N	111.1
VAL	68	H	8.2	GLU	142	N	123.0	PHE	195	H	8.5
VAL	68	HA	3.7	GLU	142	H	8.6	PHE	195	HA	4.8
VAL	68	HG1	1.3	GLU	142	HB	1.9	PHE	195	HB2	3.4
VAL	68	HG2	1.2	GLU	142	HA	3.4	PHE	195	HB3	3.2
VAL	68	HB	2.4	GLU	142	HG	1.9	GLY	196	CA	47.9
THR	69	C	177.1	ALA	143	C	178.1	GLY	196	N	107.1
THR	69	CA	65.5	ALA	143	CA	51.6	GLY	196	H	8.8
THR	69	CB	67.1	ALA	143	CB	18.6	GLY	196	HA2	4.9
THR	69	CG2	22.9	ALA	143	N	117.6	GLY	196	HA3	5.0
THR	69	N	106.2	ALA	143	H	8.7	TRP	197	C	176.7
THR	69	H	7.9	ALA	143	HA	4.4	TRP	197	CA	57.8
THR	69	HA	4.3	ALA	143	HB	1.0	TRP	197	N	119.1

THR	69	HG2	1.6	GLY	144	C	174.6	TRP	197	H	8.6
THR	69	HB	4.7	GLY	144	CA	45.8	TRP	197	HA	5.0
GLY	70	C	175.4	GLY	144	N	105.9	ALA	198	C	177.1
GLY	70	CA	48.3	GLY	144	H	7.5	ALA	198	CA	54.4
GLY	70	N	115.9	GLY	144	HA2	4.3	ALA	198	CB	18.1
GLY	70	H	8.9	GLY	144	HA3	4.1	ALA	198	N	118.7
GLY	70	HA	4.0	ILE	145	C	174.7	ALA	198	H	7.3
ILE	71	C	177.9	ILE	145	CA	63.2	ALA	198	HA	4.1
ILE	71	CA	65.5	ILE	145	CB	39.4	ALA	198	HB	2.0
ILE	71	CB	37.8	ILE	145	CD1	13.8	ILE	199	C	175.1
ILE	71	CD1	14.2	ILE	145	CG1	28.7	ILE	199	CA	61.8
ILE	71	CG2	19.0	ILE	145	CG2	17.5	ILE	199	CB	38.3
ILE	71	N	123.2	ILE	145	N	121.3	ILE	199	N	111.0
ILE	71	HA	4.1	ILE	145	H	8.3	ILE	199	H	6.8
ILE	71	H	9.3	ILE	145	HA	4.0	ILE	199	HA	3.8
ILE	71	HB	2.1	ILE	145	HB	1.8	PRO	201	C	179.0
ILE	71	HD1	1.2	ILE	145	HG2	1.1	PRO	201	CA	65.8
ILE	71	HG2	1.8	ILE	145	HD1	1.1	PRO	201	CB	30.2
ALA	72	C	178.9	ILE	145	HG1	1.3	PRO	201	CD	49.4
ALA	72	CA	55.1	MET	146	C	173.8	PRO	201	CG	27.1
ALA	72	CB	18.1	MET	146	CA	53.1	PRO	201	N	135.1
ALA	72	N	121.0	MET	146	CB	37.8	PRO	201	HG	2.3
ALA	72	H	7.6	MET	146	CG	32.0	PRO	201	HA	4.7
ALA	72	HA	4.4	MET	146	N	115.0	PRO	201	HD	4.8
ALA	72	HB	1.7	MET	146	H	7.4	PRO	201	HB	2.1
PHE	73	CA	58.2	MET	146	HA	4.9	VAL	202	C	178.0
PHE	73	CB	42.3	MET	146	HB	2.1	VAL	202	CA	67.8
PHE	73	N	120.1	MET	146	HG	3.0	VAL	202	CB	31.2
PHE	73	H	9.0	ALA	147	C	177.2	VAL	202	CG1	23.7
PHE	73	HA	4.3	ALA	147	CA	53.3	VAL	202	CG2	21.1
PHE	73	HB	2.6	ALA	147	CB	18.5	VAL	202	N	118.5
GLY	81	CA	46.4	ALA	147	N	125.5	VAL	202	H	7.5
GLY	81	N	106.8	ALA	147	H	8.9	VAL	202	HA	3.7
GLY	81	HA2	4.1	ALA	147	HA	4.5	VAL	202	HB	2.4
GLY	81	H	6.8	ALA	147	HB	1.8	VAL	202	HG1	1.3
GLY	81	HA3	4.2	ALA	148	C	181.9	VAL	202	HG2	1.1
VAL	82	CA	66.0	ALA	148	CA	55.9	GLY	203	CA	48.0
VAL	82	CB	31.8	ALA	148	CB	18.7	GLY	203	N	112.2
VAL	82	CG1	22.6	ALA	148	N	124.5	GLY	203	H	9.0
VAL	82	CG2	22.5	ALA	148	H	8.5	GLY	203	HA	4.2
VAL	82	H	7.3	ALA	148	HA	4.2	THR	206	CA	68.7
VAL	82	HA	4.2	ALA	148	HB	1.6	THR	206	CB	72.7
VAL	82	HB	2.2	TRP	149	CA	62.9	THR	206	CG2	21.6
VAL	82	HG1	1.1	TRP	149	CB	28.5	THR	206	N	105.2
VAL	82	HG2	1.2	TRP	149	CD1	130.5	THR	206	H	8.0
THR	86	CA	61.9	TRP	149	CG	113.7	THR	206	HA	4.9
THR	86	CB	72.6	TRP	149	N	118.7	THR	206	HB	4.4
THR	86	CG2	21.1	TRP	149	H	9.8	THR	206	HG2	1.3
THR	86	N	105.9	TRP	149	HA	4.3	GLY	207	CA	45.5
THR	86	H	8.3	TRP	149	HB	3.6	GLY	207	N	112.2
THR	86	HA	4.8	PRO	150	CA	66.4	GLY	207	H	8.0
THR	86	HB	4.5	PRO	150	CD	50.2	GLY	207	HA	4.4
GLY	87	C	171.0	PRO	150	N	132.4	ASN	208	CA	51.8
GLY	87	CA	45.0	PRO	150	HA	4.5	ASN	208	N	118.6
GLY	87	N	113.0	PRO	150	CG	28.0	ASN	208	H	8.3
GLY	87	H	8.2	PRO	150	CB	30.5	ILE	222	CA	65.6

GLY	87	HA	3.8	PRO	150	HG	2.2	ILE	222	N	115.7
ASP	88	C	174.7	PRO	150	HB2	2.3	ILE	222	H	7.7
ASP	88	CA	52.5	PRO	150	HD	4.2	ILE	222	HA	3.8
ASP	88	CB	43.9	PRO	150	HB3	2.5	ILE	222	CB	37.7
ASP	88	CG	180.8	ALA	151	C	178.2	ILE	222	HB	2.1
ASP	88	N	116.9	ALA	151	CA	56.5	TYR	223	CB	35.6
ASP	88	H	7.7	ALA	151	CB	18.4	TYR	223	CA	57.6
ASP	88	HA	5.0	ALA	151	N	118.2	TYR	223	HA	4.7
THR	91	C	178.3	ALA	151	H	7.5	TYR	223	HB	3.4
THR	91	CA	66.0	ALA	151	HA	4.4	TYR	223	N	118.4
THR	91	CB	67.1	ALA	151	HB	1.9	TYR	223	H	8.2
THR	91	CG2	22.9	PHE	152	CA	60.8	ASN	224	C	177.2
THR	91	N	120.0	PHE	152	CB	40.0	ASN	224	CA	55.1
THR	91	H	9.3	PHE	152	N	116.9	ASN	224	CB	36.5
THR	91	HA	4.3	PHE	152	H	7.8	ASN	224	CG	173.9
THR	91	HB	4.7	PHE	152	HA	4.1	ASN	224	N	120.0
THR	91	HG2	1.6	PHE	152	HB	3.4	ASN	224	ND2	99.4
LEU	99	C	173.3	ILE	153	CA	65.2	ASN	224	HA	5.4
LEU	99	CA	57.9	ILE	153	CB	37.6	ASN	224	HB	3.2
LEU	99	CB	42.0	ILE	153	CD1	13.1	ASN	224	H	8.3
LEU	99	CG	26.6	ILE	153	CG1	29.4	ASN	224	HD21	6.5
LEU	99	N	114.1	ILE	153	CG2	17.2	ASN	224	HD22	6.8
LEU	99	H	8.4	ILE	153	N	120.5	LEU	225	C	179.8
LEU	99	HA	4.4	ILE	153	H	8.7	LEU	225	CA	57.4
LEU	99	HG	1.2	ILE	153	HA	3.8	LEU	225	CB	41.2
LEU	99	HB	1.6	ILE	153	HB	2.3	LEU	225	CD2	22.7
LEU	99	CD1	25.8	ILE	153	HG1	1.8	LEU	225	CG	26.4
LEU	99	CD2	22.7	ILE	153	HG2	1.2	LEU	225	N	116.1
LEU	99	HD1	1.0	ILE	153	HD1	0.9	LEU	225	H	8.0
LEU	99	HD2	1.0	ILE	154	C	177.5	LEU	225	HA	4.4
LEU	100	C	178.0	ILE	154	CA	65.9	LEU	225	HG	2.3
LEU	100	CA	55.2	ILE	154	CB	37.3	LEU	225	HD2	1.0
LEU	100	CB	43.2	ILE	154	CD1	12.9	LEU	225	HB	2.3
LEU	100	CD2	22.7	ILE	154	CG1	29.4	ALA	226	C	179.9
LEU	100	CG	26.4	ILE	154	CG2	16.2	ALA	226	CA	55.0
LEU	100	HA	4.7	ILE	154	N	118.2	ALA	226	CB	18.5
LEU	100	HB	2.3	ILE	154	H	8.2	ALA	226	N	119.5
LEU	100	HG	2.2	ILE	154	HA	3.6	ALA	226	H	9.0
LEU	100	HD2	1.1	ILE	154	HG2	-0.0	ALA	226	HA	4.3
LEU	100	N	107.8	ILE	154	HG1	1.9	ALA	226	HB	1.8
LEU	100	H	7.1	ILE	154	HD1	0.8	ASP	227	C	180.6
THR	101	C	177.1	ILE	154	HB	1.5	ASP	227	CA	58.2
THR	101	CA	65.4	GLY	155	C	176.7	ASP	227	CB	40.4
THR	101	CB	70.6	GLY	155	CA	47.9	ASP	227	CG	178.1
THR	101	CG2	22.4	GLY	155	N	104.4	ASP	227	N	119.2
THR	101	N	107.6	GLY	155	H	8.5	ASP	227	H	7.7
THR	101	HA	4.5	GLY	155	HA2	3.8	ASP	227	HA	5.0
THR	101	H	8.7	GLY	155	HA3	4.1	ASP	227	HB	3.3
THR	101	HG2	1.3	SER	156	C	178.9	PHE	228	C	176.6
THR	101	HB	4.3	SER	156	CA	62.6	PHE	228	CA	63.4
VAL	102	CA	68.7	SER	156	CB	61.4	PHE	228	CB	38.4
VAL	102	CB	27.4	SER	156	N	118.3	PHE	228	N	119.8
VAL	102	CG1	23.7	SER	156	H	8.1	PHE	228	H	8.6
VAL	102	CG2	21.1	SER	156	HA	4.3	PHE	228	HA	4.4
VAL	102	N	123.5	SER	156	HB	4.3	PHE	228	HB	3.2
VAL	102	H	9.0	LEU	157	C	178.0	VAL	229	C	176.1

VAL	102	HA	4.0	LEU	157	CA	58.2	VAL	229	CA	64.5
VAL	102	HB	2.4	LEU	157	CB	41.5	VAL	229	CB	33.5
VAL	102	HG2	0.8	LEU	157	CD1	26.0	VAL	229	CG1	22.4
VAL	102	HG1	0.1	LEU	157	CD2	22.8	VAL	229	CG2	21.3
PRO	103	C	178.7	LEU	157	CG	27.0	VAL	229	N	116.9
PRO	103	CA	65.2	LEU	157	N	120.5	VAL	229	HB	2.4
PRO	103	CB	31.5	LEU	157	H	8.3	VAL	229	HG1	1.3
PRO	103	CD	51.0	LEU	157	HA	4.2	VAL	229	HG2	1.4
PRO	103	N	135.0	LEU	157	HB	2.3	VAL	229	HA	4.4
PRO	103	HA	4.7	LEU	157	HD1	1.1	VAL	229	H	7.4
PRO	103	HB	2.3	LEU	157	HD2	1.1	ASN	230	C	175.6
PRO	103	HD	3.7	LEU	157	HG	2.1	ASN	230	CA	55.0
PRO	103	CG	28.2	ALA	158	C	178.5	ASN	230	CB	38.9
PRO	103	HG	2.5	ALA	158	CA	55.6	ASN	230	CG	171.5
LEU	104	CA	58.2	ALA	158	CB	18.1	ASN	230	N	113.7
LEU	104	CB	41.5	ALA	158	N	121.2	ASN	230	ND2	108.2
LEU	104	CD1	26.4	ALA	158	H	7.9	ASN	230	H	8.8
LEU	104	CG	27.1	ALA	158	HA	4.3	ASN	230	HA	5.1
LEU	104	N	116.0	ALA	158	HB	1.7	ASN	230	HB	2.9
LEU	104	H	8.1	TRP	159	C	177.5	ASN	230	HD21	6.1
LEU	104	HA	4.1	TRP	159	CA	59.6	ASN	230	HD22	6.2
LEU	104	HB	1.8	TRP	159	CB	29.0	LYS	231	CA	59.1
LEU	104	HG	2.1	TRP	159	CD1	122.7	LYS	231	CB	35.7
LEU	104	CD2	22.7	TRP	159	CE2	139.5	LYS	231	CD	30.4
LEU	104	HD1	1.1	TRP	159	CG	110.8	LYS	231	CG	28.5
LEU	104	HD2	1.1	TRP	159	N	119.1	LYS	231	N	113.0
LEU	105	C	180.2	TRP	159	H	7.6	LYS	231	H	8.0
LEU	105	CA	58.4	TRP	159	HA	5.0	LYS	231	HA	5.2
LEU	105	CB	41.6	TRP	159	HB	3.5	LYS	231	HB	2.7
LEU	105	CD1	26.1	TYR	161	CA	62.1	LYS	231	HD	2.1
LEU	105	CD2	22.6	TYR	161	CB	37.9	LYS	231	HG	2.2
LEU	105	CG	27.1	TYR	161	CD1	132.3	ILE	232	C	176.5
LEU	105	N	119.1	TYR	161	CG	129.4	ILE	232	CA	67.4
LEU	105	H	8.9	TYR	161	N	121.1	ILE	232	CB	37.1
LEU	105	HA	4.3	TYR	161	H	8.5	ILE	232	CD1	13.9
LEU	105	HB	1.7	TYR	161	HA	4.3	ILE	232	CG1	28.8
LEU	105	HG	2.2	TYR	161	HB	3.3	ILE	232	CG2	16.2
LEU	105	HD1	1.0	MET	162	CA	60.7	ILE	232	N	119.1
LEU	105	HD2	1.1	MET	162	CB	33.8	ILE	232	H	8.8
ILE	106	C	178.8	MET	162	CG	32.2	ILE	232	HB	2.6
ILE	106	CA	61.4	MET	162	N	117.2	ILE	232	HA	4.2
ILE	106	CB	39.4	MET	162	H	7.7	ILE	232	HG2	1.1
ILE	106	CD1	14.3	MET	162	HA	3.6	ILE	232	HG1	1.3
ILE	106	CG1	31.0	MET	162	HG	2.5	ILE	232	HD1	0.8
ILE	106	CG2	20.2	MET	162	HB	1.8	LEU	233	C	177.6
ILE	106	N	117.5	ILE	163	C	177.3	LEU	233	CA	58.8
ILE	106	H	8.8	ILE	163	CA	66.4	LEU	233	CB	41.4
ILE	106	HA	4.8	ILE	163	CB	37.3	LEU	233	CD1	26.0
ILE	106	HB	2.3	ILE	163	CD1	12.0	LEU	233	CD2	25.4
ILE	106	HD1	1.2	ILE	163	CG1	28.6	LEU	233	N	119.3
ILE	106	HG1	1.3	ILE	163	CG2	17.8	LEU	233	H	8.7
ILE	106	HG2	1.1	ILE	163	N	116.9	LEU	233	HA	4.4
GLU	108	C	178.6	ILE	163	H	8.0	LEU	233	HB	1.7
GLU	108	CA	58.3	ILE	163	HA	3.3	LEU	233	CG	27.0
GLU	108	CB	28.1	ILE	163	HG1	0.4	LEU	233	HG	1.8
GLU	108	CG	30.3	ILE	163	HD1	-0.2	LEU	233	HD1	1.0

GLU	108	N	120.2	ILE	163	HB	1.8	PHE	234	CA	62.6
GLU	108	H	8.8	ILE	163	HG2	0.8	PHE	234	CB	40.9
GLU	108	HB	2.1	TYR	164	C	177.6	PHE	234	N	115.3
GLU	108	HA	5.0	TYR	164	CA	62.2	PHE	234	H	7.1
GLU	108	HG	3.0	TYR	164	CB	37.8	PHE	234	HA	4.2
PHE	109	C	177.0	TYR	164	N	120.2	PHE	234	HB2	3.0
PHE	109	CA	63.6	TYR	164	H	9.0	PHE	234	HB3	3.4
PHE	109	CB	39.2	TYR	164	HA	4.3	GLY	235	C	176.3
PHE	109	N	115.6	TYR	164	HB	3.2	GLY	235	CA	47.6
PHE	109	H	7.9	GLU	165	C	178.8	GLY	235	N	100.8
PHE	109	HA	4.3	LEU	166	C	178.0	GLY	235	H	7.3
PHE	109	HB	3.4	LEU	166	CA	55.6	GLY	235	HA2	3.9
TYR	110	C	175.7	LEU	166	HA	4.4	GLY	235	HA3	4.2
TYR	110	CA	62.1	TRP	167	C	177.1	LEU	236	C	179.1
TYR	110	CB	38.5	TRP	167	CA	59.5	LEU	236	CA	58.3
TYR	110	N	114.4	TRP	167	CB	30.3	LEU	236	CB	42.1
TYR	110	H	7.2	TRP	167	N	121.3	LEU	236	CD1	26.6
TYR	110	HA	4.5	TRP	167	HA	4.5	LEU	236	CD2	23.5
TYR	110	HB	3.2	TRP	167	H	9.3	LEU	236	CG	27.3
LEU	111	C	180.7	TRP	167	HB	2.3	LEU	236	N	123.7
LEU	111	CA	58.4	ALA	168	C	177.1	LEU	236	H	8.8
LEU	111	CB	41.6	ALA	168	CA	51.7	LEU	236	HA	5.0
LEU	111	CD1	25.5	ALA	168	CB	22.4	LEU	236	HD2	0.7
LEU	111	CD2	23.0	ALA	168	N	117.5	LEU	236	HG	1.8
LEU	111	N	118.3	ALA	168	H	8.7	LEU	236	HB	1.8
LEU	111	H	8.9	ALA	168	HA	4.7	ILE	237	C	178.5
LEU	111	HA	4.0	ALA	168	HB	1.4	ILE	237	CA	64.7
LEU	111	CG	27.1	GLY	169	C	174.5	ILE	237	CB	37.1
ILE	112	C	176.9	GLY	169	CA	44.7	ILE	237	CG1	29.0
ILE	112	CA	64.5	GLY	169	N	109.3	ILE	237	CG2	17.8
ILE	112	CB	38.2	GLY	169	H	7.5	ILE	237	N	121.6
ILE	112	CD1	13.7	GLY	169	HA	3.5	ILE	237	H	8.4
ILE	112	CG1	29.7	GLU	170	C	179.3	ILE	237	HA	4.0
ILE	112	CG2	17.4	GLU	170	CA	59.6	ILE	237	HB	2.4
ILE	112	N	114.0	GLU	170	CB	30.4	ILE	237	HG2	1.2
ILE	112	H	9.0	GLU	170	CG	35.0	ILE	237	HG1	1.9
ILE	112	HA	4.3	GLU	170	N	125.5	ILE	237	CD1	13.8
ILE	112	HB	2.0	GLU	170	H	9.3	ILE	237	HD1	1.1
ILE	112	HG2	1.3	GLU	170	HA	4.3	ILE	238	C	176.5
ILE	112	HD1	1.1	GLU	170	HB	1.7	ILE	238	CA	65.0
ILE	112	HG1	1.6	GLU	170	HG	2.3	ILE	238	CB	37.4
LEU	113	C	178.8	GLY	171	C	174.3	ILE	238	CD1	14.7
LEU	113	CA	57.3	GLY	171	CA	47.8	ILE	238	CG1	29.4
LEU	113	CB	41.3	GLY	171	N	105.6	ILE	238	CG2	17.2
LEU	113	CD1	25.2	GLY	171	H	8.3	ILE	238	N	122.4
LEU	113	CD2	22.9	GLY	171	HA	3.9	ILE	238	H	7.1
LEU	113	CG	26.4	LYS	172	C	178.3	ILE	238	HA	3.8
LEU	113	N	119.5	LYS	172	CA	56.9	ILE	238	HB	2.3
LEU	113	H	7.0	LYS	172	CB	30.2	ILE	238	HD1	0.8
LEU	113	HA	4.3	LYS	172	CD	27.2	ILE	238	HG2	1.1
LEU	113	HG	1.1	LYS	172	CG	23.5	TRP	239	C	175.5
LEU	113	HB	2.2	LYS	172	N	122.8	TRP	239	CA	62.6
LEU	113	HD1	1.0	LYS	172	H	6.5	TRP	239	CB	28.5
ALA	114	C	179.1	LYS	172	HA	4.1	TRP	239	CG	110.7
ALA	114	CA	53.9	LYS	172	HB	1.8	TRP	239	N	119.8
ALA	114	CB	16.5	LYS	172	HG	1.3	TRP	239	H	9.0

ALA	114	N	122.8	SER	173	C	176.7	TRP	239	HA	4.3
ALA	114	H	8.9	SER	173	CA	61.7	TRP	239	HB2	3.7
ALA	114	HA	4.2	SER	173	CB	62.7	TRP	239	HB3	4.2
ALA	114	HB	1.1	SER	173	N	113.1	ASN	240	C	176.7
ALA	115	C	177.5	SER	173	H	8.3	ASN	240	CA	57.1
ALA	115	CA	53.4	SER	173	HA	4.3	ASN	240	CB	40.0
ALA	115	CB	15.5	SER	173	HB	4.2	ASN	240	CG	174.7
ALA	115	N	118.6	ALA	174	C	180.1	ASN	240	N	114.4
ALA	115	H	7.0	ALA	174	CA	54.6	ASN	240	H	8.7
ALA	115	HA	3.9	ALA	174	CB	18.8	ASN	240	HA	3.7
ALA	115	HB	-0.0	ALA	174	N	121.8	ASN	240	HB	3.1
ALA	116	C	177.5	ALA	174	H	7.6	VAL	241	C	174.5
ALA	116	CA	53.0	ALA	174	HA	4.6	VAL	241	CA	64.4
ALA	116	CB	23.8	ALA	174	HB	1.8	VAL	241	CB	30.7
ALA	116	N	117.9	SER	175	C	175.9	VAL	241	CG1	25.1
ALA	116	H	7.3	SER	175	CA	62.1	VAL	241	CG2	19.4
ALA	116	HA	4.8	SER	175	CB	62.5	VAL	241	N	117.7
ALA	116	HB	2.0	SER	175	N	117.7	VAL	241	H	7.8
THR	117	N	114.8	SER	175	H	8.8	VAL	241	HB	2.2
THR	117	H	8.7	SER	175	HA	3.8	VAL	241	HG2	1.2
THR	117	CA	59.1	SER	175	HB	4.2	VAL	241	HA	4.0
THR	117	HA	4.9	ASN	176	C	176.1	VAL	241	HG1	1.0
LYS	126	C	178.4	ASN	176	CA	54.8	ALA	242	C	180.6
LYS	126	CA	60.5	ASN	176	CB	38.4	ALA	242	CA	54.4
LYS	126	CB	34.1	ASN	176	CG	175.7	ALA	242	CB	19.5
LYS	126	CD	30.4	ASN	176	N	117.5	ALA	242	N	126.3
LYS	126	CE	42.7	ASN	176	ND2	110.8	ALA	242	H	8.2
LYS	126	CG	26.6	ASN	176	H	7.6	ALA	242	HA	2.3
LYS	126	N	116.8	ASN	176	HA	4.7	ALA	242	HB	1.5
LYS	126	NZ	33.4	ASN	176	HB	3.1	VAL	243	CA	66.7
LYS	126	H	8.1	ASN	176	HD22	6.8	VAL	243	N	119.7
LYS	126	HA	4.1	ASN	176	HD21	7.5	VAL	243	H	8.2
LYS	126	HB	1.8	THR	177	C	173.8	VAL	243	HA	3.4
LEU	127	C	178.6	THR	177	CA	61.4	VAL	243	CB	31.2
LEU	127	CA	57.5	THR	177	CB	70.1	VAL	243	HB	2.2
LEU	127	CB	41.4	THR	177	CG2	21.4	LYS	244	CA	59.9
LEU	127	CD2	20.5	THR	177	N	107.3	LYS	244	N	121.9
LEU	127	CG	26.1	THR	177	H	7.8	LYS	244	HA	4.1
LEU	127	N	115.7	THR	177	HA	4.8	LYS	244	H	7.8
LEU	127	H	7.6	THR	177	HB	4.8	LYS	244	CB	32.1
LEU	127	HA	4.3	THR	177	HG2	1.6	LYS	244	HB	2.0
LEU	127	HB	2.4	ALA	178	C	175.9	LYS	244	CG	25.1
LEU	127	HG	1.1	ALA	178	CA	50.4	LYS	244	HG	1.7
LEU	128	CA	58.3	ALA	178	CB	20.7	ASN	248	C	172.3
LEU	128	CB	41.7	ALA	178	N	124.9	ASN	248	CA	52.5
LEU	128	CD1	26.8	ALA	178	H	7.6	ASN	248	CB	39.1
LEU	128	CD2	23.5	ALA	178	HA	4.8	ASN	248	N	118.8
LEU	128	CG	27.2	ALA	178	HB	1.7	ASN	248	H	8.4
LEU	128	N	120.3	SER	179	C	172.9	ASN	248	HA	5.2
LEU	128	H	8.5	SER	179	CA	56.9	ASN	248	HB	3.0
LEU	128	HA	4.3	SER	179	CB	62.5	ALA	249	CA	51.9
LEU	128	HB2	1.8	SER	179	N	117.1	ALA	249	CB	20.9
LEU	128	HG	2.1	SER	179	H	8.5	ALA	249	N	130.6
				SER	179	HA	5.0	ALA	249	H	9.0
				SER	179	HB2	4.4	ALA	249	HA	5.0
				SER	179	HB3	4.8	ALA	249	HB	1.9

References

(1) Barbet-Massin, E.; Pell, A. J.; Retel, J. S.; Andreas, L. B.; Jaudzems, K.; Franks, W. T.; Nieuwkoop, A. J.; Hiller, M.; Higman, V.; Guerry, P.; Bertarello, A.; Knight, M. J.; Felletti, M.; Le Marchand, T.; Kotelovica, S.; Akopjana, I.; Tars, K.; Stoppini, M.; Bellotti, V.; Bolognesi, M.; Ricagno, S.; Chou, J. J.; Griffin, R. G.; Oschkinat, H.; Lesage, A.; Emsley, L.; Herrmann, T.; Pintacuda, G. *J. Am. Chem. Soc.* **2014**, *136*, 12489-12497.

(2) Stanek, J.; Andreas, L. B.; Jaudzems, K.; Cala, D.; Lalli, D.; Bertarello, A.; Schubeis, T.; Akopjana, I.; Kotelovica, S.; Tars, K.; Pica, A.; Leone, S.; Picone, D.; Xu, Z. Q.; Dixon, N. E.; Martinez, D.; Berbon, M.; El Mammeri, N.; Noubhani, A.; Saupe, S.; Habenstein, B.; Loquet, A.; Pintacuda, G. *Angew. Chem. Int. Ed. Engl.* **2016**, *55*, 15504-15509.

(3) Karaca, E.; Melquiond, A. S.; de Vries, S. J.; Kastritis, P. L.; Bonvin, A. M. *Mol Cell Proteomics* **2010**, *9*, 1784-1794.

(4) Bennett, A. E. R., C. M.; Auger, M.; Lakshmi, K. V.; Griffin, R. G. *J. Chem. Phys.* **1995**, *103*, 6951-6958.